HHS Public Access

Author manuscript

J Physiol. Author manuscript; available in PMC 2023 November 02.

Published in final edited form as:

J Physiol. 2023 October ; 601(19): 4291–4308. doi:10.1113/JP284690.

Oncomodulin Regulates Spontaneous Calcium Signaling and Maturation of Afferent Innervation in Cochlear Outer Hair Cells

Yang Yang[1], **Kaitlin Murtha**[1], **Leslie K. Climer**[1], **Federico Ceriani**[2], **Pierce Thompson**[1], **Aubrey J. Hornak**[1], **Walter Marcotti**[2,4], **Dwayne D. Simmons**[1,2,3,5,#]

[1]Department of Biology, Baylor University, 101 Bagby Ave, Waco, TX

[2]School of Biosciences, University of Sheffield, S10 2TN Sheffield, United Kingdom

[3]Department of Integrative Biology and Physiology, University of California, Los Angeles, CA

[4]Sheffield Neuroscience Institute, University of Sheffield, Sheffield, S10 2TN, UK

[5]Department of Psychology and Neuroscience, Baylor University, Waco, TX

Abstract

Cochlear outer hair cells (OHCs) are responsible for the exquisite frequency selectivity and sensitivity of mammalian hearing. During development, the maturation of OHC afferent connectivity is refined by coordinated spontaneous Ca^{2+} activity in both sensory and non-sensory cells. Calcium signaling in neonatal OHCs can be modulated by oncomodulin (OCM, β-parvalbumin), an EF-hand calcium-binding protein. Here, we investigated whether OCM regulates OHC spontaneous Ca^{2+} activity and afferent connectivity during development. Using a genetically encoded Ca^{2+} sensor (GCaMP6s) expressed in OHCs in wild-type (*Ocm*$^{+/+}$) and *Ocm* knockout (*Ocm*$^{-/-}$) littermates, we found increased spontaneous Ca^{2+} activity and upregulation of purinergic receptors in OHCs from *Ocm*$^{-/-}$ cochlea immediately following birth. The afferent synaptic maturation of OHCs was delayed in the absence of OCM, leading to an increased number of ribbon synapses and afferent fibers on *Ocm*$^{-/-}$ OHCs before hearing onset. We propose that OCM regulates the spontaneous Ca^{2+} signaling in the developing cochlea and the maturation of OHC afferent innervation.

[#]To whom correspondence should be addressed: dwayne_simmons@baylor.edu.

Competing interests

The authors declare no conflicts of interest.

CRediT authorship contribution statement

Yang Yang: Formal Analysis, Investigation, Methodology, Software, Visualization, Writing – original draft, Writing – review & editing. **Kaitlin E. Murtha**: Investigation, Methodology, Writing – review & editing. **Leslie K. Climer**: Methodology, Validation, Writing – review & editing. **Federico Ceriani**: Methodology, Validation, Formal analysis, Writing – review & editing. **Pierce Thompson**: Investigation, Methodology, Writing – review & editing. **Aubrey J. Hornak**: Project administration, Investigation, Writing – review & editing. **Walter Marcotti**: Conceptualization, Methodology, Software, Resources, Writing – review & editing, Supervision, Project administration, Funding acquisition. **Dwayne D. Simmons**: Conceptualization, Methodology, Formal analysis, Investigation, Resources, Data curation, Writing – original draft, Writing – review & editing, Visualization, Supervision, Project administration, Funding acquisition.

All authors approved the final version of the paper. All authors agree to be accountable for all aspects of the work in ensuring that questions related to the accuracy or integrity of any part of the work are appropriately investigated and resolved. All persons designated as authors qualify for authorship, and all those who qualify for authorship are listed.

Keywords

Oncomodulin (OCM); Outer Hair Cell (OHC); Purinergic receptors; Presynaptic ribbons; Spontaneous Calcium activity; Voltage-gated Calcium channels; EF-hand Calcium binding protein

Introduction

The regulation and control of Ca^{2+} is a major challenge for cochlear sensory cells during development as well as in the adult. Similar to other sensory systems, the developing cochlea exhibits intrinsically generated, sound-independent spontaneous Ca^{2+} activity that is critical for the maturation and refinement of neural circuits (Lippe, 1994; Blankenship & Feller, 2010; Clause *et al.*, 2014; Babola *et al.*, 2021). The mammalian cochlea has two types of specialized sensory cells, which are involved in the transduction of sound into electrical responses (Dallos, 1992). Inner hair cells (IHCs) relay sounds information via glutaminergic synapses onto type I afferent spiral ganglion neurons. Outer hair cells (OHCs) enhance cochlear sensitivity and frequency tuning of the cochlear partition and are primarily innervated by cholinergic medial olivocochlear neurons that form a sound-evoked acoustic reflex (Guinan, 2018). Additionally, OHCs form synapses onto type II afferent spiral ganglion neurons that may be activated by traumatic noise exposures (Flores *et al.*, 2015; Liu *et al.*, 2015). In rodents, the maturation of OHC innervation patterns occurs during the first and second postnatal weeks (Simmons, 1994; Simmons *et al.*, 1996). Recent studies show that the OHC innervation is refined by coordinated spontaneous Ca^{2+} activity. Ca^{2+} waves initiated in the greater epithelial ridge (GER), or Kölliker's organ, a developmentally transient structure located adjacent to the row of IHCs, synchronize the spontaneous Ca^{2+} activity in OHCs through the modulation of voltage-gated Ca^{2+} channels and purinergic receptor signaling (Ceriani *et al.*, 2019; Jeng *et al.*, 2020). However, little is known about the intracellular Ca^{2+} signaling network that modulates OHC spontaneous Ca^{2+} activity during cochlear maturation.

A multitude of transporters, pumps, exchangers, and calcium-binding proteins (CaBPs) are integral to the Ca^{2+} signaling network in OHCs and tightly regulate Ca^{2+} activity and homeostasis. Oncomodulin (OCM), a small EF-hand CaBP of approximately 12 kDa, is the β isoform of parvalbumin and shares at least 53% sequence identity with α-parvalbumin (PVALB) (Banville & Boie, 1989). Previous studies show that in the cochlea, OCM is expressed specifically by OHCs and preferentially localizes to the lateral membrane, the basal portion of the hair bundle, and the basal pole adjacent to efferent terminals (Simmons *et al.*, 2010). After hearing onset, which in most altricial rodents occurs at around postnatal day 12 (P12), OHCs express high levels of OCM (2–3 mM) compared to other CaBPs (Hackney *et al.*, 2005). Together, this suggests that OCM may have a special function relative to the other CaBPs in OHCs. OCM is an important CaBP for which targeted deletion causes hearing loss (Pangrsic *et al.*, 2015; Tong *et al.*, 2016). The absence of OCM alters Ca^{2+} signaling in OHCs before the onset of hearing (Murtha *et al.*, 2022), revealing a major role of OCM in regulating Ca^{2+} activity during maturation. Given that spontaneous Ca^{2+} activity plays a critical role in OHC development, we hypothesized that OCM modulates spontaneous Ca^{2+} activity during development.

To investigate how OCM regulates spontaneous Ca^{2+} activity in developing OHCs, we expressed a genetically encoded, tissue-specific Ca^{2+} sensor (*Atoh1*-GCaMP6s) in *Ocm* wild-type ($Ocm^{+/+}$) and *Ocm* knockout ($Ocm^{-/-}$) mice. $Ocm^{-/-}$ mice exhibited early onset hearing loss, and their OHCs showed faster KCl-induced Ca^{2+} transients than those recorded from $Ocm^{+/+}$ mice and other mouse strains (Tong *et al.*, 2016; Climer *et al.*, 2021; Murtha *et al.*, 2022). In neonatal mice (P2), we observed spontaneous Ca^{2+} activity in OHCs that was synchronized by Ca^{2+} waves elicited in the GER. However, $Ocm^{-/-}$ OHCs exhibited higher synchronization and stronger fractional change of GCaMP6s fluorescence intensity ($\Delta F/F_0$) during Ca^{2+} activity in the GER, compared to $Ocm^{+/+}$ OHCs. We also found that the expression of P2X2, one of the main purinergic receptors in the cochlea, was upregulated in $Ocm^{-/-}$ cochlea. $Ocm^{-/-}$ OHCs showed delayed synaptic pruning with an increased number of tunnel crossing fibers during development. We propose that the lack of OCM alters the spontaneous Ca^{2+} activity via ATP signaling and affects the afferent maturation and innervation of the OHCs.

Materials and Methods

Ethical approval

Animals were bred at the Baylor University Vivarium. The animal work was licensed by the Institutional Animal Care and Use Committee (IACUC), Baylor University as established by U.S. Public Health Service.

Animals

All mouse colonies were purchased from the Jackson Laboratory. For these studies, *Atoh1*-GCaMP6s mouse lines were maintained on mixed backgrounds. We first crossed *Ocm* wildtype ($Ocm^{+/+}$) and *Ocm* knockout ($Ocm^{-/-}$) mice with B6;129S-*Gt(ROSA)26Sor*$^{tm96.1(CAG-GCaMP6s)Hze}$/J, Ai96(RCL-GCaMP6s) or Ai96, which contains a floxed-STOP cassette preventing transcription of the GCaMP6 slow variant Ca^{2+} indicator. These mice were then crossed with knock-in transgenic mice expressing Cre recombined from the *Atoh1* locus (Chen *et al.*, 2013). *Atoh1*-driven Cre GCaMP6s mice showed tissue-specific expression of endogenous green fluorescence (Yang *et al.*, 2010; Cox *et al.*, 2012; Mulvaney & Dabdoub, 2012). We utilized GCaMP6s positive $Ocm^{+/+}$ and $Ocm^{-/-}$ mice to monitor intracellular Ca^{2+} activities directly after acute dissection.

Cochlear Function Assays

For measurement of distortion product otoacoustic emissions (DPOAEs), adult mice were anesthetized with xylazine (20 mg/kg, i.p.) and ketamine (100 mg/kg, i.p.). Acoustic stimuli were delivered using a custom acoustic assembly previously described (Maison *et al.*, 2012). Briefly, two electrostatic earphones (EC-1, Tucker Davis Technologies) were used to generate primary tones and a Knowles miniature microphone (EK-3103) was used to record ear-canal sound pressure. Stimuli were generated digitally with 4 s sampling. Ear-canal sound pressure and electrode voltage were amplified and digitally sampled at 20s for analysis of response amplitudes. Both outputs and inputs were processed with a digital I-O board (National Instruments PXI-4461). For measurement of DPOAEs at 2f1 – f2, the primary tones were set so that the frequency ratio, (f2/f1), was 1.2 and so that f2 level was

10 dB below f1 level. For each f2/f1 primary pair, levels were swept in 10 dB steps from 20 dB SPL to 80 dB SPL (for f2). At each level, both waveform and spectral averaging were used to increase the signal-to-noise ratio of the recorded ear-canal sound pressure, and the amplitude of the DPOAE at 2f1 – f2 was extracted from the averaged spectra, along with the noise floor at nearby points in the spectrum. Iso-response curves were interpolated from plots of DPOAE amplitude vs. sound level. The threshold was defined as the f2 level required to produce a DPOAE at 0 dB SPL. Right ears were used for all hearing tests.

Tissue preparation

Cochleae were harvested from *Ocm*$^{+/+}$ or *Ocm*$^{-/-}$ mice of either sex at postnatal day 2 (P2), P6, P10, and 3 – 4 weeks as previously described (Murtha *et al.*, 2022). Briefly, pups were euthanized by rapid induction of hypothermia, and apical coil OHCs were dissected from the organ of Corti in an extracellular medium composed of (in mM): 136.8 NaCl, 5.4 KCl, 0.4 KH_2PO_4, 0.3 Na_2HPO_4, 0.8 $MgSO_4$, 1.3 $CaCl_2$, 4.2 $NaHCO_3$, 5 HEPES and 5.6 glucose. The pH was adjusted to 7.4 – 7.5 (osmolality ~306 mmol/kg). The apical coil was then transferred to a small microscope chamber with nylon mesh fixed to a stainless-steel ring on the bottom and visualized using an upright microscope (Leica, DM 6000 FS, Germany) with a 63x / 0.90 water immersion long working distance objective (Leica, 15506362 HCX APO L 63x/0.90 W U-V-I CS2).

Confocal Ca^{2+} imaging

Ca^{2+} signals from GCaMP6s were recorded using a spinning disk confocal microscope system containing X-Light V2 spinning disk confocal (89 North Inc.) and PRIME95B Photometrics Cooled sCMOS with 95% QE (1200 ×1200 pixels with 792 dpi, Teledyne photometric). Images were analyzed offline using ImageJ (NIH). Ca^{2+} signals were measured as relative changes of fluorescence emission intensity ($\Delta F/F_0$) and calculated by MATLAB. $\Delta F = F - F_0$, where F is fluorescence at time t and F_0 is the fluorescence at the onset of the recording.

For spontaneous Ca^{2+} activity, GCaMP6s positive cochlea was recorded immediately after acute dissection at room temperature with 480nm excitation wavelength. Each GCaMP6s fluorescence recording consisted of 1103 frames taken at 6 frames per second from 912 ×912 pixels region, 80 ms exposure time. Fluorescence traces were computed as pixel averages from each OHC ROI and $\Delta F/F_0$ was calculated in MATLAB. The average GCaMP6s fluorescence of the first 50 frames was used as baseline (F_0). A Savitzky-Golay filter was then applied to smooth the $\Delta F/F_0$ and increase the signal-to-noise ratio of Ca^{2+} signals (window length = 11, polynomial order = 1). A spike inference algorithm in MATLAB was used to estimate the spike count and position. Only the peak above 4 standard deviations of baseline was calculated ($F_0 + 4 \times SD$, shown as dash line in Figure 4 and Figure 5). The minimum peak distance was 5 frames. The average frequency was then computed by dividing the number of spikes by the total duration of the recording. For the spontaneous activity in the GER, the ROI was drawn around the maximum area of each multicellular Ca^{2+} event, and the maximum longitudinal extension of calcium event in non-sensory cells was then measured with ImageJ and a stage micrometer calibration slide (Olympus, Japan). We calculated the pairwise Spearman's rank correlation coefficient (r_s)

between every pair of OHCs in the field of view during the spontaneous Ca^{2+} waves in the GER (time window 2), or during the absence of Ca^{2+} activity in the GER (time window 1). The significance was tested using Mann-Whitney U-test (one-sided). The average of Spearman's rank correlation coefficient (r_{avg}) was calculated from r_s after Fisher's z-transformation:

$$z = \text{arctanh}(r_s)$$

$$r_{avg} = \tanh(z)$$

r_{avg} was then used for the liner regression with corresponding extension size along the cochlear spiral, *f-test* was used to determine if the slope is significantly non-zero.

KCl depolarization solution contained (in mM): 142.4 KCl, 0.4 KH_2PO_4, 0.3 Na_2HPO_4, 0.8 $MgSO_4$, 1.3 $CaCl_2$, 4.2 $NaHCO_3$, 5 HEPES and 5.6 glucose. The pH was adjusted to 7.4 – 7.5 (osmolality ~305 mmol/kg). ATP depolarization solution was diluted from 100 mM stock ATP (Thermo Fisher Scientific, USA) with the extracellular solution (800 μM ATP for working solution). PPADS (Sigma, USA) and nifedipine (Sigma, USA) were dissolved with DMSO and then diluted using the extracellular solution. Ca^{2+}-free medium composed of (in mM): 136.8 NaCl, 5.4 KCl, 0.4 KH_2PO_4, 0.3 Na_2HPO_4, 0.8 $MgSO_4$, 4.2 $NaHCO_3$, 5 HEPES, 5.6 glucose with 1 EGTA. The pH was adjusted to 7.4 – 7.5 (osmolality ~306 mmol/kg). Depolarization solution was delivered to the chamber using a PMD-D35 perfusion/media exchange system (Tokai Hit, Japan), followed by 2 min perfusion with the extracellular solution.

For Ca^{2+} transients, 100 μl of KCl depolarization solution, or 100 μl of ATP depolarization solution was added into a microscope chamber containing 300 μl extracellular solution (1:4 dilution, ~40 μM K^+ final concentration, or 200 μM ATP final concentration in the chamber). For the nifedipine or PPADS experiments, the blocker was added to the explant right before ATP or KCl application. The perfusion system (Tokai Hit, Japan) started 8 s after the imaging started without generating any turbulence. We measured Ca^{2+} fluorescence from activated OHCs (reach maximum fluorescence intensity between 8–60 s) from all trials separately to avoid the disturbance from spontaneous Ca^{2+} activity.

Each Ca^{2+} fluorescence recording includes 1500 frames taken at 80 frames per second using VisiView (VISITRON, USA). After background subtraction, the activated OHCs were computed as pixel averages using ImageJ. Calcium transient time constant (τ) was determined

Genotyping and qRT-PCR

DNA was extracted from mice tail samples using Extract-N-Amp™ Tissue PCR Kit (Sigma, USA). PCR primers used for genotyping are listed below: *Atoh1*-Cre primer pair forward: 5'- CCGGCAGAGTTTACAGAAGC-3', reverse: 5'-ATG TTT AGC TGG CCC AAA TG-3'; Cre control primer pair forward: 5'-CTA GGC CAC AGA ATT GAA AGA

TCT-3’; reverse: 5’-GTA GGT GGA AAT TCT AGC ATC ATC C-3’; GCaMP6s primer pair forward: 5’- ACG AGT CGG ATC TCC CTT TG - 3’; reverse: 5’- AGA CTG CCT TGG GAA AAG CG - 3’; *Ocm* primer pair forward: 5’- CTC CAC ACT TCA CCA AGC AG - 3’, reverse: 5’- TTT CAT GTT CAG GGA TCA AGT G - 3’; *Ocm* deletion primer pair forward: 5’- CTC CAC ACT TCA CCA AGC AG - 3’, reverse: 5’- GCT TGG GGA CCC CCT GTC TTC A - 3’.

Bilateral cochleae were acutely dissected after anesthesia and transferred to the lysis buffer. Total RNA was extracted using RNeasy plus Micro kits (QIAGEN, USA). iScript™ Advanced cDNA Synthesis Kit (Bio-Rad, USA) was used for reverse transcription.

qRT-PCR was performed using the SYBR Green PCR Master Mix Kit (Bio-Rad, USA) as previously described (Murtha *et al.*, 2022). Briefly, the *b2m* gene was used as a reference gene (Melgar-Rojas *et al.*, 2015). Quantification of expression (fold change) from the Cq data was calculated following the ΔΔCq method (Schmittgen & Livak, 2008), and normalized to the Cq value in $Ocm^{+/+}$ at P0. $2^{-\Delta\Delta Cq}$ was calculated to represent the relative expression (fold change).

Primers used for qRT-PCR are as follows: *b2m* forward 5’-TGGTCTTTCTGGTGCTTGTC-3’ and reverse 5’-GGG TGG AAC TGT GTT ACG TAG-3’; *Ocm* forward 5’- ATG AGC ATC ACG GAC ATT CTG AGC-3’ and reverse 5’-CTG GCA GAC ATC TTG GAG AGG C-3’; *CACNA1D* forward 5’- GCA AAC TAT GCA AGA GGC ACC AGA C −3’ and reverse 5’- CTT TGG GAG AGA GAT CCT ACA GGT G −3’; *P2RX2* forward 5’- GCG TTC TGG GAC TAC GAG AC −3’ and reverse 5’- ACG TAC CAC ACG AAG TAA AGC −3’ (PrimerBank ID 27544798a1). *P2RX3* forward 5’- CAA CAC AAC AAG TTT GAA CCC AGC −3’ and reverse 5’- AGG CTT CTT TAG CTT CTC ACTG −3’, *P2RX7* forward 5’- CCC TGC ACA GTG AAC GAG TA −3’ and reverse 5’-CGT GGA GAG ATA GGG ACA GC −3’.

Immunofluorescence microscopy

Histological analysis and immunocytochemistry were applied as previously described (Murtha *et al.*, 2022). Briefly, cochleae from neonatal mice were flushed with 4% PFA and then fixative overnight at 4°C, followed by 3 washes in PBS, then blocked in 5% normal horse serum (NHS) for 1 h at room temperature. Samples were stained with antibodies to OCM (Santa Cruz Biotechnology, USA, sc-7446, 1:200), P2X2 (Alomone Labs, Israel, APR-003, 1:400), the C-terminal-binding protein 2 (CtBP2, BD Biosciences #612044, 1:200) and peripherin (Sigma, USA, AB1530, 1:200). Primary antibodies were incubated overnight at 37°C. Appropriate Alexa Fluor (Thermo Scientific, USA, 1:200) and Northern Lights (R&D Systems 1:200) conjugated secondary antibodies were incubated for 1 hour at 37°C. Slides were prepared using Vectashield mounting media with DAPI (Vector Laboratories, USA). Images were acquired using the LSM800 microscope (Zeiss, Germany) using a high-resolution, oil-immersion objective (Plan-Apochromat 63x, 1.4 NA). Cohorts of samples were immunostained at the same time and imaged under the same optical conditions to allow for direct comparison.

Western Blotting

Dissected cochleae were harvested (3 cochleae in the same tube, total n = 9 for each genotype) and immediately placed into a lysis buffer containing: 1% Triton X-100, 25 mM Tris, pH 7.4, 150 mM NaCl, 1 mm DTT, 1 mm $MgCl_2$, 1 mM phenylmethylsulfonyl fluoride, and 1x protease inhibitor cocktail (Thermo Scientific, USA). Samples were incubated on ice for 10 minutes and vigorously vortexed twice in 15 second intervals. Lysates were spun down at 4°C 12,000 x g for 20 minutes. Total protein concentration was determined using a BCA Protein Assay Kit (Pierce, ThermoFisher Scientific, USA). The supernatant was diluted in sample buffer (Bio-Rad, USA, 355 mM β-ME added) and heated for 30 minutes at 37°C. Samples (25 μg total protein) were subject to SDS-PAGE and protein was transferred to a PVDF membrane. Membranes were blocked with 2.5% fish gelatin for 1 hour at RT and incubated overnight at 4°C with primary antibody to rabbit P2X2R (1:400; Alomone Labs, Israel), mouse $Ca_v1.3$ (1:100; ThermoFisher Scientific, USA), and rabbit β-tubulin (1:1000). After washing, membranes were incubated with appropriate HRP-conjugated secondaries (anti-rabbit 1:7,500, anti-mouse 1:100) for 1 hour at RT. Clarity Max ECL Substrate (Bio-Rad USA) was used to detect chemiluminescence via a ChemiDoc imaging system. Relative protein expression levels (normalized to β-tubulin) were determined by densitometric analysis using FIJI software.

Statistical analysis

Statistical analysis was performed using GraphPad Prism 9 and MATLAB software. Statistical comparisons of means were made by t-test or, when normal distribution could not be assumed, the *Mann-Whitney U*-test. For multiple comparisons, *one-way* or *two-way ANOVA* followed by *Bonferroni* post test was used. Data is given as mean ± SD. Animals of either sex were randomly assigned to the different experimental groups. No statistical methods were used to define the sample size, which was selected based on previously published similar work from our laboratories. Animals were taken from multiple cages and breeding pairs.

Results

Lack of OCM expression causes early hearing loss in GCaMP6s adult mice

We utilized tissue-specific expression of GCaMP6s (Figure 1A) to investigate Ca^{2+} signaling in the cochlea. *Atoh1*-driven Cre mice were crossed with the Ai96 mice containing a floxed-STOP cassette GCaMP6s. *Atoh1* expression is found in IHCs and OHCs during development (Mulvaney & Dabdoub, 2012). As a sensitive GFP-based Ca^{2+} sensor, GCaMP6s has been used to probe fast Ca^{2+} dynamics and low peak Ca^{2+} accumulations in neurons (Chen *et al.*, 2013; Lukasz & Kindt, 2018; Shilling-Scrivo *et al.*, 2021). Compared to other variants, GCaMP6 sensors have similar baseline fluorescence but a higher dynamic range (1.1 – 1.6 fold increase compared to GCaMP5G) and larger signals (>10-fold compared to GCaMP3)(Chen *et al.*, 2013). Because of all the above features, we probed Ca^{2+} signaling in the OHCs using GCaMP6s *Ocm* control ($Ocm^{+/+}$) and *Ocm* knockout ($Ocm^{-/-}$) mice (Figure 1A). Initially, we examined OHC function in adult *Ocm* mice expressing GCaMP6s by measuring distortion product otoacoustic emissions (DPOAEs). At 3 – 4 weeks (wks), there were no differences in DPOAE thresholds between $Ocm^{+/+}$ and

Ocm$^{-/-}$ mice (Figure 1B). However, by 7 – 9 wks, *Ocm*$^{-/-}$ mice showed hearing loss with higher DPOAE thresholds at 16, 22, and 32 kHz ($P = 0.007$, *two-way ANOVA*, Figure 1C). These results are consistent with other studies showing that OCM is critical for maintaining cochlear function in adult mice (Tong *et al.*, 2016; Climer *et al.*, 2021).

In the cochlea of *Ocm*$^{+/+}$ mice, *Ocm* mRNA was detected as early as P0 and was significantly upregulated at P2. Relative *Ocm* mRNA expression in *Ocm*$^{-/-}$ cochlea was negligible compared to that of *Ocm*$^{+/+}$ (Figure 1D, $P < 0.001$, *one-way ANOVA*). Using confocal microscopy, we found that at P2 both *Ocm*$^{+/+}$ and *Ocm*$^{-/-}$ mice showed endogenous GCaMP6s fluorescence in the cochlea (Figure 1E). OHCs from *Ocm*$^{-/-}$ mice exhibited higher baseline fluorescence intensity compared to those in control mice (F_0, Figure 1E), indicating a possible higher basal level of intracellular Ca^{2+} due to the lack of OCM as previously suggested (Murtha *et al.*, 2022). OCM was also differentially expressed along the tonotopic axis of the cochlea, being higher towards the base of the cochlea (Figure 1F).

The absence of OCM changes Ca^{2+} signaling in the postnatal development of Ocm$^{-/-}$ mice

Changes in intracellular Ca^{2+} induced by extracellular KCl caused increases in GCaMP6s fluorescence in OHCs (Figure 2A,Movie 1), as previously demonstrated (Murtha *et al.*, 2022). The change in Ca^{2+} levels in OHCs from all 3 rows was probed by the fractional change in signal fluorescence ($\Delta F/F_0$, Figure 2B). OHCs from *Ocm*$^{-/-}$ mice showed significantly increased average maximum $\Delta F/F_0$ compared *Ocm*$^{+/+}$ OHCs ($P < 0.001$, *t*-test, Figure 2C). The time course of the Ca^{2+} transient induced by extracellular KCl in *Ocm*$^{-/-}$ OHCs exhibited a faster rise-time constant compared to *Ocm*$^{+/+}$ OHCs at P2 (Figure 2D). As a Ca^{2+} binding protein, GCaMP6s could alter Ca^{2+} buffering in OHCs. However, GCaMP6s was present in OHCs from both control and *Ocm*$^{-/-}$ mice, and Ca^{2+} activity in *Ocm*$^{+/+}$ OHCs was similar to that previously measured in non-GCaMP6s transgenic mice (Murtha *et al.*, 2022). We then sought to verify whether the KCl-induced Ca^{2+} transients depend on voltage-gated Ca^{2+} channels. In both *Ocm*$^{+/+}$ and *Ocm*$^{-/-}$ OHCs, Ca^{2+} transients were nearly eliminated when KCl was applied together with 250 μM nifedipine (Figure 2E), and average maximum $\Delta F/F_0$ was comparable in OHCs from both genotypes (maximum $\Delta F/F_0$ without normalization: 0.396 ± 0.175 for *Ocm*$^{+/+}$ mice, 0.448 ± 0.249 for *Ocm*$^{-/-}$ mice, $P = 0.153$, *t*-test). A dose-response curve, normalized to $\Delta F/F_0$ with 250 μM nifedipine, showed that KCl-induced Ca^{2+} transients were partially blocked by 10 or 50 μM of the Ca^{2+} channel blocker ($P < 0.001$, *two-way ANOVA*, Figure 2F). Since the $Ca_v1.3$ channel is the main voltage-gated L-type Ca^{2+} channel expressed in hair cells (Platzer *et al.*, 2000; Michna *et al.*, 2003), we investigated whether the lack of OCM altered their expression. qRT-PCR showed that the relative $Ca_v1.3$ mRNA expression (encoded by *CACNA1D*) in the cochlea of P2 *Ocm*$^{-/-}$ mice was significantly downregulated compared to of control mice ($P = 0.003$, *t*-test, Figure 2G). Western blot also showed that the *Ocm*$^{-/-}$ cochlea exhibited a significantly lower level of $Ca_v1.3$ protein compared to *Ocm*$^{+/+}$ cochlea ($P = 0.049$. *t*-test, Figure 2H–I).

Targeted deletion of Ocm increased spontaneous calcium signaling in the immature cochlea

During early postnatal development, OHCs show spontaneous Ca^{2+} activity that can be synchronized by ATP-induced Ca^{2+} waves originating from the GER, and depends on extracellular Ca^{2+} via $Ca_v1.3$ channel (Ceriani *et al.*, 2019; Jeng *et al.*, 2020). Since we recently showed that OCM expression alters intracellular Ca^{2+} signaling in OHCs (Murtha et al., 2022), we hypothesized that the absence of OCM in *Ocm*$^{-/-}$ mice could affect the spontaneous Ca^{2+} activity in the OHCs. Apical OHCs from both *Ocm*$^{+/+}$ and *Ocm*$^{-/-}$ P2 mice showed increased coordination of Ca^{2+} activity during the occurrence of a Ca^{2+} wave in the GER (time window 2, yellow), compared to when there were no Ca^{2+} waves (time window 1, green, Figure 3A–F, Movie 2). Spontaneous Ca^{2+} activity was nearly eliminated in a Ca^{2+}-free medium (with 1mM EGTA), and in the presence of 250 μM nifedipine, indicating that spontaneous Ca^{2+} activity in OHCs depends on extracellular Ca^{2+}. To quantify the synchronization of Ca^{2+} signals in OHCs with Ca^{2+} waves in the GER, the average pairwise correlation coefficient between OHC Ca^{2+} traces was calculated in the time window during the occurrence of Ca^{2+} waves in the GER (r_{avg}). For OHCs, the r_{avg} from both *Ocm*$^{+/+}$ and *Ocm*$^{-/-}$ mice showed a positive relationship with the longitudinal extension size of Ca^{2+} events in the GER and was significantly different from zero (Figure 4A, $P < 0.001$ for *Ocm*$^{+/+}$ and *Ocm*$^{-/-}$, *t*-test). There was no significant difference between the average extension sizes of Ca^{2+} waves in the GER from *Ocm*$^{+/+}$ and *Ocm*$^{-/-}$ mice (*Ocm*$^{+/+}$: 85.50 ± 61.00 μm, *Ocm*$^{-/-}$: 95.90 ± 60.70 μm, $P = 0.193$, *t*-test). These results indicate that the lack of OCM in OHCs did not change the positive relationship between the extension size of Ca^{2+} waves in the GER and the correlation coefficient (Ceriani *et al.*, 2019). Correlation coefficients displayed a monotonic relationship with the Ca^{2+} wave longitudinal extension. Fitting this relationship with linear regression yielded a steeper slope for *Ocm*$^{-/-}$ compared to *Ocm*$^{+/+}$ (4.39 ± 0.93 nm^{-1} vs. 2.66 ± 0.88 nm^{-1}, $P = 0.008$, *t*-test, Figure 4A). We calculated the mean r_{avg} in OHCs, *Ocm*$^{-/-}$ OHCs exhibited a significantly increased mean r_{avg} compared to *Ocm*$^{+/+}$ OHCs ($P = 0.006$, *Mann-Whitney* test, Figure 4B). We then calculated the average maximum $\Delta F/F_0$ for each Ca^{2+} spike in OHCs (Figure 4C–D). During spontaneous Ca^{2+} waves, the average maximum $\Delta F/F_0$ in *Ocm*$^{-/-}$ OHCs was greater than in *Ocm*$^{+/+}$ OHCs (Figure 4D, $P < 0.001$, *Mann-Whitney* test). Altogether, we found that similar-sized Ca^{2+} waves from the GER produced increased synchronization and higher average maximum $\Delta F/F_0$ of spontaneous Ca^{2+} activity in the OHCs of *Ocm*$^{-/-}$ relative to those in *Ocm*$^{+/+}$ mice.

Lack of OCM expression increases ATP-induced Ca^{2+} signaling and purinergic receptors expression in cochlear OHCs

ATP signaling plays a central role during the development of the cochlea. Cochlear cells exhibit a diverse array of purinergic signaling components including all subtypes of ionotropic P2X and metabotropic P2Y receptor subunits (Housley *et al.*, 2009). In the immature cochlea, OHCs express P2X and P2Y receptors and exhibit depolarizing, ATP-gated currents (Glowatzki *et al.*, 1997; Bobbin, 2001). Initially, we investigated whether purinergic signaling is altered in the absence of OCM, by investigating whether spontaneous Ca^{2+} activity in OHCs was blocked by the ionotropic P2X purinergic receptor antagonist PPADS (100 μM). Both *Ocm*$^{+/+}$ and *Ocm*$^{-/-}$ OHCs showed spontaneous Ca^{2+} activity

(Figure 5A, C). However, in the presence of PPADS, the Ca^{2+} waves originating from the GER failed to synchronize the Ca^{2+} signaling in OHCs ($P > 0.999$, *Mann-Whitney U*-test, time window 1 vs. time window 2, Figure 5B, D). The presence of PPADS also affected the linear relationship between the extension size of Ca^{2+} waves in GER and the r_{avg} in both $Ocm^{+/+}$ and $Ocm^{-/-}$ OHCs (Figure 5E). However, the average maximum $\Delta F/F_0$ of spontaneous spikes was significantly decreased only in $Ocm^{-/-}$ OHCs (Figure 5G, $P < 0.001$ *two-way ANOVA*).

We then investigated whether Ca^{2+} transients in OHCs elicited by extracellular ATP were affected in the absence of OCM at P2. $Ocm^{-/-}$ OHCs showed significantly higher maximum $\Delta F/F_0$ signal compared to $Ocm^{+/+}$ mice (Figure 6A–C, $P < 0.001$, *t*-test). ATP-induced Ca^{2+} transients in $Ocm^{-/-}$ OHCs were nearly eliminated in Ca^{2+}-free medium (with 1mM EGTA, the average of maximum $\Delta F/F_0$: 0.664 ± 0.495, 43 OHCs from 2 mice). The Ca^{2+} activity was abolished in OHCs when ATP was applied with the presence of 100 μM PPADS (the average of maximum $\Delta F/F_0$: 0.351 ± 0.142, 35 OHCs from 2 mice). Altogether, these data indicate that purinergic signaling can modulate spontaneous Ca^{2+} activity in both $Ocm^{+/+}$ and $Ocm^{-/-}$ OHCs. Since the lack of OCM causes a larger Ca^{2+} response induced by ATP in OHCs similar to KCl, we investigated whether there were changes in the expression of P2X receptors. Among known P2X receptors, P2X2, P2X3, and P2X7 are all expressed in the cochlea during development (Housley *et al.*, 1998; Nikolic *et al.*, 2003; Huang *et al.*, 2006). We performed qRT-PCR on cochlea harvested from $Ocm^{+/+}$ and $Ocm^{-/-}$ mice at P2. *P2RX2*, *P2RX3*, and *P2RX7* mRNA expression were significantly higher in $Ocm^{-/-}$ cochlea compared to $Ocm^{+/+}$ cochlea (Figure 7A, *P2RX2* $P = 0.021$, *P2RX3*, $P < 0.001$ and *P2RX7*, $P = 0.028$, *t*-test). However, *P2RX2* receptor expression demonstrated the greatest fold change among the three purinergic receptors (> 10 fold) in OHCs from $Ocm^{-/-}$ mice compared with littermate controls. Western blot revealed that $Ocm^{-/-}$ cochlea showed significantly upregulated P2X2 protein expression relative to $Ocm^{+/+}$ (Figure 7B, $P = 0.026$, *t*-test), which was further supported by immunofluorescence experiments (Figure 7C).

The number of afferent fibers in $Ocm^{-/-}$ mice is increased

In the cochlea, the type II afferent fibers cross the tunnel and contact multiple OHCs, and form branches to the outer supporting cells, including Deiter's cells and Hensen's cells (Fechner *et al.*, 2001). The maturation of synaptic contacts includes a transformation from multiple small to one single presynaptic active zone (Michanski *et al.*, 2019). Thus, we expected that the changes in spontaneous Ca^{2+} activity might affect ribbon synapse maturation and afferent innervation in $Ocm^{-/-}$ OHCs. We first counted the number of afferent ribbons in OHC from pre- and post-hearing $Ocm^{+/+}$ and $Ocm^{-/-}$ mice. The number of CtBP2 puncta in OHCs increased between P2 and P6 in both $Ocm^{+/+}$ and $Ocm^{-/-}$ mice. Between P6 and P10 there was a drastic reduction of puncta in $Ocm^{+/+}$ mice, but not in $Ocm^{-/-}$ mice. However, by 3 – 4 wks, the number of ribbons labeled by CtBP2 in $Ocm^{+/+}$ and $Ocm^{-/-}$ apical cochlea showed no significant difference (Figure 8A–E, $P = 0.004$ *two-way ANOVA*, P2, $P > 0.999$, P6, $P > 0.999$, P10, $P < 0.001$, 3 – 4 wks, $P > 0.999$, *Bonferroni* post test). Our results suggested that the synaptic maturation and pruning in $Ocm^{-/-}$ cochlea was delayed compared to $Ocm^{+/+}$ cochlea. We then used peripherin to examine type II afferent spiral ganglion (SG) fibers (Hafidi, 1998) in cochleae from $Ocm^{+/+}$

and *Ocm*$^{-/-}$ mice at P6 and P10 (Figure 9A, B). The SG neurons formed outer spiral fibers that terminate on OHCs after long spiral courses. Peripherin immunofluorescence revealed that *Ocm*$^{-/-}$ mice showed a similar number of tunnel crossing fibers compared to *Ocm*$^{+/+}$ mice at P6 (Figure 9C, $P = 0.375$, *t*-test), but had an increased number of tunnel crossing fibers compared to *Ocm*$^{+/+}$ mice at P10 (Figure 9D, $P = 0.002$, *t*-test). These data provide evidence that the increased spontaneous Ca^{2+} signaling in *Ocm*$^{-/-}$ cochlea changes the maturation of afferent synapses and innervation of afferent fibers during development.

Discussion

In the present study, we showed that OCM influences the development of spontaneous activity in OHCs and modulates their neonatal afferent innervation. We generated *Ocm*$^{+/+}$ and *Ocm*$^{-/-}$ mice with a genetically encoded calcium sensor (GCaMP6s). Similar to other studies (Tong *et al.*, 2016; Climer *et al.*, 2021), *Ocm*$^{-/-}$ mice showed normal hearing at 3 – 4 weeks of age but exhibited an early onset hearing loss at 7–9 weeks. Compared to *Ocm*$^{+/+}$ mice, OHCs from P2 *Ocm*$^{-/-}$ mice have higher maximum $\Delta F/F_0$ GCaMP6s fluorescence intensity induced by ATP and KCl, which is consistent with higher levels of free cytosolic Ca^{2+} as previously reported (Murtha *et al.*, 2022). Both *Ocm*$^{+/+}$ and *Ocm*$^{-/-}$ OHCs exhibited spontaneous Ca^{2+} activity that is synchronized by Ca^{2+} waves initiated from the GER. However, OHCs from *Ocm*$^{-/-}$ mice had an increased level of coordinated spontaneous Ca^{2+} activity compared to littermate controls. Further, *Ocm*$^{-/-}$ OHCs exhibited an increased number of presynaptic ribbons and afferent tunnel-crossing fibers just prior to the onset of the hearing. Taken together OCM contributes to the modulation of Ca^{2+} signaling and the maturation of afferent connectivity in the developing mouse cochlea.

OCM modulates the expression of Ca^{2+}-related genes during development

Purinergic receptors have been implicated in auditory neurotransmission, regulation of cochlear homeostasis, cochlear development, and neurodegenerative conditions (Housley *et al.*, 2009; Burnstock, 2016; Linden *et al.*, 2019). Previous studies have shown that all P2X receptors are transiently expressed in the developing mammalian cochlea (Vlajkovic & Thorne, 2022). Among these purinergic receptors, P2X3 and P2X7 are expressed in sensory hair cells from embryonic day 18 (E18) to P6 (Nikolic *et al.*, 2003; Huang *et al.*, 2006). P2X2 receptors are the predominant purinergic receptor in the mature cochlea and is expressed in hair cells before P15 (Jarlebark *et al.*, 2002). We found that the expression of P2X2, P2X3, and P2X7 purinergic receptors were all upregulated due to the lack of OCM. The upregulation of P2X receptors in the *Ocm*$^{-/-}$ cochlea could be explained either by an OCM-mediated regulatory pathway or by the effect of Ca^{2+} levels on purinergic reveptors expression. Several studies suggest CaBPs may interact directly with purinergic receptors. Roger et al. (2008) found that P2X7 receptors contain a large intracellular C-terminal domain with a Ca^{2+}-dependent calmodulin (CaM) binding motif. Moreover, the Ca^{2+}-CaM binding motif changes the conformation of P2X7, indicating a possible intracellular regulatory pathway of P2X7 receptors (Sander et al., 2022). Since OCM and CaM share some functional similarities (MacManus *et al.*, 1982; Climer *et al.*, 2019), it is possible that OCM may interact with P2X receptors to alter their function and expression. Alternatively, upregulated purinergic receptors could be associated with

the higher concentrations of cytosolic free Ca^{2+} in *Ocm*$^{-/-}$ OHCs. Loss of OCM or noise exposure has been shown to cause increased levels of intracellular free Ca^{2+}, leading to Ca^{2+} overloading in OHCs (Zuo *et al.*, 2008; Murtha *et al.*, 2022). Noise exposure also leads to the upregulation of P2X receptors in sensory hair cells (Wang *et al.*, 2003). Thus, the loss of OCM could lead to unrestrained P2X function and increased expression either because of the loss of a direct regulator, or through unfettered cytosolic free Ca^{2+}.

Unlike the upregulation of P2X receptors, we found that the expression of $Ca_v1.3$, which is the predominant voltage-gated Ca^{2+} channel in hair cells (Michna *et al.*, 2003; Hafidi & Dulon, 2004), was downregulated in the *Ocm*$^{-/-}$ cochlea. Spontaneous Ca^{2+} activity in OHCs is dependent upon the expression of $Ca_v1.3$ channels (Ceriani *et al.*, 2019; Jeng *et al.*, 2020). Although there is little evidence for CaBPs directly modulating $Ca_v1.3$ expression, previous studies show that CaBPs can modulate $Ca_v1.3$ activity. CaM modulates $Ca_v1.3$ channel open probability based on cytosolic Ca^{2+} levels (Johny *et al.*, 2013). CaM increases the activity of $Ca_v1.3$ channels at low cytosolic Ca^{2+} levels, and decreases the permeability of $Ca_v1.3$ channels at high Ca^{2+} levels. Additionally, other CaBPs (e.g., CaBP1, CaBP2, CaBP3, and CaBP4) enhance Ca^{2+} feedback to $Ca_v1.3$ channels (Cui *et al.*, 2007). Similar to other CaBPs, OCM could potentially modulate the function of $Ca_v1.3$ channels. In this way, the expression of OCM or the downregulation of Ca^{2+} entry prevents Ca^{2+} overloading in OHCs and protects them from cytotoxicity. Indeed, mice lacking $Ca_v1.2$, another voltage-gated Ca^{2+} channel expressed in hair cells, reduces vulnerability to noise (Zuccotti *et al.*, 2013). The progressive hearing loss phenotype observed in *Ocm*$^{-/-}$ mice could be the result of the insufficiency of protective mechanisms in *Ocm*$^{-/-}$ OHCs to reduce intracellular Ca^{2+} and thus protect mice from hearing loss.

Taken together, our data suggest that OCM regulates the expression of two purinergic receptors and $Ca_v1.3$ channels during the early stages of development. Therefore, OCM may contribute significantly to shaping Ca^{2+} dynamics, a cornerstone of auditory hair cell function. Since noise leads to changes in Ca^{2+} activity and Ca^{2+}-related gene expression, OCM could play a key role in preventing OHC damage due to noise exposure.

Lack of OCM alters spontaneous Ca^{2+} activity and afferent maturation in OHC

Our data show that OHCs from pre-hearing *Ocm*$^{-/-}$ mice exhibited higher synchronized Ca^{2+} activity compared to OHCs from littermate control mice. Spontaneous Ca^{2+} waves are generated from the GER and travel to the lesser epithelial ridge (LER), where the OHCs are located. Deiters' cells in LER synchronize the Ca^{2+} activity in nearby OHCs via the release of ATP (Ceriani *et al.*, 2019). Interestingly, the expression of OCM in OHCs increases during development (Hackney *et al.*, 2005; Simmons *et al.*, 2010), and parallels the downregulation of spontaneous Ca^{2+} activity in developing OHCs (Ceriani *et al.*, 2019; Jeng *et al.*, 2020). In the present study, we found a gradient expression of OCM in OHCs along the tonotopic axis of the cochlea. Indeed, spontaneous Ca^{2+} activity is higher in apical compared to basal OHCs at early postnatal ages (Lelli *et al.*, 2009; Ceriani *et al.*, 2019; Jeng *et al.*, 2020). These studies support the idea that OCM regulates spontaneous Ca^{2+} activity during the maturation of OHCs. Both $Ca_v1.3$ Ca^{2+} channels and purinergic receptor channels are thought to modulate spontaneous Ca^{2+} activity in developing OHCs. We found

The lack of OCM down-regulates the $Ca_V1.3$ expression, but up-regulates the ATP receptor expression. In OHCs from *Ocm*$^{-/-}$ mice, the larger Ca^{2+} transients during spontaneous Ca^{2+} activity in OHCs from is due to, at least partly, the upregulation of ATP receptors, while the down-regulation of $Ca_V1.3$ could be a compensatory mechanism of Ca^{2+} overloading caused by the lack of OCM.

During the early postanal period, Ca^{2+} influxes and periodic Ca^{2+} stimulation are required for synaptic maturation and afferent refinement (Balland *et al.*, 2006; Spitzer, 2006; Tritsch *et al.*, 2007; Sheets *et al.*, 2012). Recent studies suggest that coordinated Ca^{2+} activity in OHCs is necessary for the formation of their afferent connectivity. The reduction of synchronized spontaneous Ca^{2+} activity in the connexin 30 knockout (*Cx30*$^{-/-}$) OHCs results in a decreased number of ribbon synapses and type II afferent fibers (Ceriani *et al.*, 2019; Jeng *et al.*, 2020). Here, we found that a higher level of spontaneous Ca^{2+} activity increases the number of synaptic ribbons and type II afferent fibers. These data reveal that similar to *Cx30*$^{-/-}$, OCM-regulated spontaneous Ca^{2+} activity is also critical to the early patterns of synaptic maturation and afferent innervation during cochlear development. We also found that the increased number of ribbons did not persist in the adult mice. Since several studies have shown that a high percentage of type II afferent terminals are not associated with OHC presynaptic ribbons (Liberman *et al.*, 1990; Weisz *et al.*, 2012; Martinez-Monedero *et al.*, 2016; Vyas *et al.*, 2017), the number of type II afferent fibers in adult mice needs further investigation. Type II afferents have been suggested as cochlear nociceptors to detect tissue damage (Flores *et al.*, 2015; Liu *et al.*, 2015), thus, if higher numbers of type II afferents persist in adult *Ocm*$^{-/-}$, they could have a higher sensitivity to noise exposure.

In summary, the lack of OCM downregulates $Ca_V1.3$ channels in OHCs and upregulates P2X2 receptors in the cochlea. Without OCM expression at P2, spontaneous Ca^{2+} activity in OHCs is higher and more synchronized with the GER. We conclude that the lack of OCM changes Ca^{2+} signaling in immature OHCs, resulting in delayed synaptic pruning and changed afferent innervation during the pre-hearing period. We propose that OCM prevents Ca^{2+} overloading and regulates Ca^{2+} signaling necessary for the correct synaptic maturation and afferent innervation during development.

Funding

This work was supported by National Institute on Deafness and Other Communication Disorders Grants DC013304 and DC018935 (DDS), American Hearing Research Foundation grant 2021, and the BBSRC BB/T004991/1 (WM).

Data Availability Statement:

The data that support the findings of this study are available from the corresponding author upon reasonable request.

References

Babola TA, Li S, Wang Z, Kersbergen CJ, Elgoyhen AB, Coate TM & Bergles DE. (2021). Purinergic Signaling Controls Spontaneous Activity in the Auditory System throughout Early Development. J Neurosci 41, 594–612. [PubMed: 33303678]

Balland B, Lachamp P, Strube C, Kessler J-P & Tell F. (2006). Glutamatergic synapses in the rat nucleus tractus solitarii develop by direct insertion of calcium-impermeable AMPA receptors and without activation of NMDA receptors. The Journal of Physiology 574, 245–261. [PubMed: 16690712]

Banville D & Boie Y. (1989). Retroviral long terminal repeat is the promoter of the gene encoding the tumor-associated calcium-binding protein oncomodulin in the rat. J Mol Biol 207, 481–490. [PubMed: 2474657]

Blankenship AG & Feller MB. (2010). Mechanisms underlying spontaneous patterned activity in developing neural circuits. Nature Reviews Neuroscience 11, 18–29. [PubMed: 19953103]

Bobbin RP. (2001). ATP-induced movement of the stalks of isolated cochlear Deiters' cells. Neuroreport 12, 2923–2926. [PubMed: 11588604]

Burnstock G (2016). P2X ion channel receptors and inflammation. Purinergic Signalling 12, 59–67. [PubMed: 26739702]

Ceriani F, Hendry A, Jeng JY, Johnson SL, Stephani F, Olt J, Holley MC, Mammano F, Engel J, Kros CJ, Simmons DD & Marcotti W. (2019). Coordinated calcium signalling in cochlear sensory and non-sensory cells refines afferent innervation of outer hair cells. EMBO J 38.

Chen T-W, Wardill TJ, Sun Y, Pulver SR, Renninger SL, Baohan A, Schreiter ER, Kerr RA, Orger MB, Jayaraman V, Looger LL, Svoboda K & Kim DS. (2013). Ultrasensitive fluorescent proteins for imaging neuronal activity. Nature 499, 295–300. [PubMed: 23868258]

Clause A, Kim G, Sonntag M, Weisz CJ, Vetter DE, Rubsamen R & Kandler K. (2014). The precise temporal pattern of prehearing spontaneous activity is necessary for tonotopic map refinement. Neuron 82, 822–835. [PubMed: 24853941]

Climer LK, Cox AM, Reynolds TJ & Simmons DD. (2019). Oncomodulin: The Enigmatic Parvalbumin Protein. Frontiers in Molecular Neuroscience 12.

Climer LK, Hornak AJ, Murtha K, Yang Y, Cox AM, Simpson PL, Le A & Simmons DD. (2021). Deletion of Oncomodulin Gives Rise to Early Progressive Cochlear Dysfunction in C57 and CBA Mice. Front Aging Neurosci 13, 749729. [PubMed: 34867279]

Cox BC, Liu Z, Lagarde MMM & Zuo J. (2012). Conditional Gene Expression in the Mouse Inner Ear Using Cre-loxP. Journal of the Association for Research in Otolaryngology 13, 295–322. [PubMed: 22526732]

Cui G, Meyer AC, Calin-Jageman I, Neef J, Haeseleer F, Moser T & Lee A. (2007). Ca2+-binding proteins tune Ca2+-feedback to Cav1.3 channels in mouse auditory hair cells. J Physiol 585, 791–803. [PubMed: 17947313]

Dallos P (1992). The active cochlea. J Neurosci 12, 4575–4585. [PubMed: 1464757]

Fechner FP, Nadol JJ, Burgess BJ & Brown MC. (2001). Innervation of supporting cells in the apical turns of the guinea pig cochlea is from type II afferent fibers. J Comp Neurol 429, 289–298. [PubMed: 11116221]

Flores EN, Duggan A, Madathany T, Hogan AK, Marquez FG, Kumar G, Seal RP, Edwards RH, Liberman MC & Garcia-Anoveros J. (2015). A non-canonical pathway from cochlea to brain signals tissue-damaging noise. Curr Biol 25, 606–612. [PubMed: 25639244]

Glowatzki E, Ruppersberg JP, Zenner HP & Rusch A. (1997). Mechanically and ATP-induced currents of mouse outer hair cells are independent and differentially blocked by d-tubocurarine. Neuropharmacology 36, 1269–1275. [PubMed: 9364481]

Guinan JJ, Jr. (2018). Olivocochlear efferents: Their action, effects, measurement and uses, and the impact of the new conception of cochlear mechanical responses. Hear Res 362, 38–47. [PubMed: 29291948]

Hackney CM, Mahendrasingam S, Penn A & Fettiplace R. (2005). The concentrations of calcium buffering proteins in mammalian cochlear hair cells. J Neurosci 25, 7867–7875. [PubMed: 16120789]

Hafidi A (1998). Peripherin-like immunoreactivity in type II spiral ganglion cell body and projections. Brain Res 805, 181–190. [PubMed: 9733963]

Hafidi A & Dulon D. (2004). Developmental expression of Cav1.3 (α1d) calcium channels in the mouse inner ear. Developmental Brain Research 150, 167–175. [PubMed: 15158080]

Housley GD, Bringmann A & Reichenbach A. (2009). Purinergic signaling in special senses. Trends Neurosci 32, 128–141. [PubMed: 19232752]

Housley GD, Luo L & Ryan AF. (1998). Localization of mRNA encoding the P2X2 receptor subunit of the adenosine 5'-triphosphate-gated ion channel in the adult and developing rat inner ear by in situ hybridization. J Comp Neurol 393, 403–414. [PubMed: 9550147]

Huang LC, Ryan AF, Cockayne DA & Housley GD. (2006). Developmentally regulated expression of the P2X3 receptor in the mouse cochlea. Histochem Cell Biol 125, 681–692. [PubMed: 16341871]

Jarlebark LE, Housley GD, Raybould NP, Vlajkovic S & Thorne PR. (2002). ATP-gated ion channels assembled from P2X2 receptor subunits in the mouse cochlea. Neuroreport 13, 1979–1984. [PubMed: 12395104]

Jeng JY, Ceriani F, Hendry A, Johnson SL, Yen P, Simmons DD, Kros CJ & Marcotti W. (2020). Hair cell maturation is differentially regulated along the tonotopic axis of the mammalian cochlea. The Journal of Physiology 598, 151–170. [PubMed: 31661723]

Johny MB, Yang PS, Bazzazi H & Yue DT. (2013). Dynamic switching of calmodulin interactions underlies Ca2+ regulation of CaV1.3 channels. Nature Communications 4, 1717.

Kim S-H, Bahia PK, Patil M, Sutton S, Sowells I, Hadley SH, Kollarik M & Taylor-Clark TE. (2020). Development of a Mouse Reporter Strain for the Purinergic P2X2 Receptor. eneuro 7, ENEURO.0203–0220.

Köles L, Szepesy J, Berekméri E & Zelles T. (2019). Purinergic Signaling and Cochlear Injury-Targeting the Immune System? International Journal of Molecular Sciences 20, 2979. [PubMed: 31216722]

Lelli A, Asai Y, Forge A, Holt JR & Geleoc GS. (2009). Tonotopic gradient in the developmental acquisition of sensory transduction in outer hair cells of the mouse cochlea. J Neurophysiol 101, 2961–2973. [PubMed: 19339464]

Liberman MC, Dodds LW & Pierce S. (1990). Afferent and efferent innervation of the cat cochlea: quantitative analysis with light and electron microscopy. J Comp Neurol 301, 443–460. [PubMed: 2262601]

Linden J, Koch-Nolte F & Dahl G. (2019). Purine Release, Metabolism, and Signaling in the Inflammatory Response. Annual Review of Immunology 37, 325–347.

Lippe W (1994). Rhythmic spontaneous activity in the developing avian auditory system. The Journal of Neuroscience 14, 1486–1495. [PubMed: 8126550]

Liu C, Glowatzki E & Fuchs PA. (2015). Unmyelinated type II afferent neurons report cochlear damage. Proc Natl Acad Sci U S A 112, 14723–14727. [PubMed: 26553995]

Lukasz D & Kindt KS. (2018). In Vivo Calcium Imaging of Lateral-line Hair Cells in Larval Zebrafish. Journal of Visualized Experiments.

MacManus JP, Whitfield JF, Boynton AL, Durkin JP & Swierenga SH. (1982). Oncomodulin--a widely distributed, tumour-specific, calcium-binding protein. Oncodev Biol Med 3, 79–90. [PubMed: 7122257]

Maison SF, Liu XP, Eatock RA, Sibley DR, Grandy DK & Liberman MC. (2012). Dopaminergic signaling in the cochlea: receptor expression patterns and deletion phenotypes. J Neurosci 32, 344–355. [PubMed: 22219295]

Martinez-Monedero R, Liu C, Weisz C, Vyas P, Fuchs PA & Glowatzki E. (2016). GluA2-Containing AMPA Receptors Distinguish Ribbon-Associated from Ribbonless Afferent Contacts on Rat Cochlear Hair Cells. eNeuro 3.

Melgar-Rojas P, Alvarado JC, Fuentes-Santamaria V, Gabaldon-Ull MC & Juiz JM. (2015). Validation of Reference Genes for RT-qPCR Analysis in Noise-Induced Hearing Loss: A Study in Wistar Rat. PLoS One 10, e0138027. [PubMed: 26366995]

Michanski S, Smaluch K, Steyer AM, Chakrabarti R, Setz C, Oestreicher D, Fischer C, Möbius W, Moser T, Vogl C & Wichmann C. (2019). Mapping developmental maturation of inner hair cell ribbon synapses in the apical mouse cochlea. Proceedings of the National Academy of Sciences 116, 6415–6424.

Michna M, Knirsch M, Hoda JC, Muenkner S, Langer P, Platzer J, Striessnig J & Engel J. (2003). Cav1.3 (α1D) Ca2+ Currents in Neonatal Outer Hair Cells of Mice. The Journal of Physiology 553, 747–758. [PubMed: 14514878]

Mulvaney J & Dabdoub A. (2012). Atoh1, an Essential Transcription Factor in Neurogenesis and Intestinal and Inner Ear Development: Function, Regulation, and Context Dependency. Journal of the Association for Research in Otolaryngology 13, 281–293. [PubMed: 22370966]

Murtha KE, Yang Y, Ceriani F, Jeng JY, Climer LK, Jones F, Charles J, Devana SK, Hornak AJ, Marcotti W & Simmons DD. (2022). Oncomodulin (OCM) uniquely regulates calcium signaling in neonatal cochlear outer hair cells. Cell Calcium 105, 102613. [PubMed: 35797824]

Nikolic P, Housley GD & Thorne PR. (2003). Expression of the P2X7 receptor subunit of the adenosine 5'-triphosphate-gated ion channel in the developing and adult rat cochlea. Audiol Neurootol 8, 28–37. [PubMed: 12566690]

Pangrsic T, Gabrielaitis M, Michanski S, Schwaller B, Wolf F, Strenzke N & Moser T. (2015). EF-hand protein Ca2+ buffers regulate Ca2+ influx and exocytosis in sensory hair cells. Proc Natl Acad Sci U S A 112, E1028–1037. [PubMed: 25691754]

Platzer J, Engel J, Schrott-Fischer A, Stephan K, Bova S, Chen H, Zheng H & Striessnig J. (2000). Congenital deafness and sinoatrial node dysfunction in mice lacking class D L-type Ca2+ channels. Cell 102, 89–97. [PubMed: 10929716]

Roger S, Pelegrin P & Surprenant A. (2008). Facilitation of P2X7 Receptor Currents and Membrane Blebbing via Constitutive and Dynamic Calmodulin Binding. Journal of Neuroscience 28, 6393–6401. [PubMed: 18562610]

Sander S, Müller I, Garcia-Alai MM, Nicke A & Tidow H. (2022). New insights into P2X7 receptor regulation: Ca2+-calmodulin and GDP bind to the soluble P2X7 ballast domain. Journal of Biological Chemistry 298, 102495. [PubMed: 36115462]

Schmittgen TD & Livak KJ. (2008). Analyzing real-time PCR data by the comparative C(T) method. Nat Protoc 3, 1101–1108. [PubMed: 18546601]

Sheets L, Kindt KS & Nicolson T. (2012). Presynaptic CaV1.3 Channels Regulate Synaptic Ribbon Size and Are Required for Synaptic Maintenance in Sensory Hair Cells. Journal of Neuroscience 32, 17273–17286. [PubMed: 23197719]

Shilling-Scrivo K, Mittelstadt J & Kanold PO. (2021). Altered Response Dynamics and Increased Population Correlation to Tonal Stimuli Embedded in Noise in Aging Auditory Cortex. J Neurosci 41, 9650–9668. [PubMed: 34611028]

Simmons DD. (1994). A transient afferent innervation of outer hair cells in the postnatal cochlea. Neuroreport 5, 1309–1312. [PubMed: 7919186]

Simmons DD, Mansdorf NB & Kim JH. (1996). Olivocochlear innervation of inner and outer hair cells during postnatal maturation: evidence for a waiting period. J Comp Neurol 370, 551–562. [PubMed: 8807454]

Simmons DD, Tong B, Schrader AD & Hornak AJ. (2010). Oncomodulin identifies different hair cell types in the mammalian inner ear. J Comp Neurol 518, 3785–3802. [PubMed: 20653034]

Spitzer NC. (2006). Electrical activity in early neuronal development. Nature 444, 707–712. [PubMed: 17151658]

Tong B, Hornak AJ, Maison SF, Ohlemiller KK, Liberman MC & Simmons DD. (2016). Oncomodulin, an EF-Hand Ca2+ Buffer, Is Critical for Maintaining Cochlear Function in Mice. J Neurosci 36, 1631–1635. [PubMed: 26843644]

Tritsch NX, Yi E, Gale JE, Glowatzki E & Bergles DE. (2007). The origin of spontaneous activity in the developing auditory system. Nature 450, 50–55. [PubMed: 17972875]

Vlajkovic SM & Thorne PR. (2022). Purinergic Signalling in the Cochlea. International Journal of Molecular Sciences 23, 14874. [PubMed: 36499200]

Vyas P, Wu JS, Zimmerman A, Fuchs P & Glowatzki E. (2017). Tyrosine Hydroxylase Expression in Type II Cochlear Afferents in Mice. J Assoc Res Otolaryngol 18, 139–151. [PubMed: 27696081]

Wang JC, Raybould NP, Luo L, Ryan AF, Cannell MB, Thorne PR & Housley GD. (2003). Noise induces up-regulation of P2X2 receptor subunit of ATP-gated ion channels in the rat cochlea. Neuroreport 14, 817–823. [PubMed: 12858039]

Weisz CJ, Lehar M, Hiel H, Glowatzki E & Fuchs PA. (2012). Synaptic transfer from outer hair cells to type II afferent fibers in the rat cochlea. J Neurosci 32, 9528–9536. [PubMed: 22787038]

Yang H, Xie X, Deng M, Chen X & Gan L. (2010). Generation and characterization of Atoh1-Cre knock-in mouse line. Genesis 48, 407–413. [PubMed: 20533400]

Zuccotti A, Lee SC, Campanelli D, Singer W, Satheesh SV, Patriarchi T, Geisler H-S, Köpschall I, Rohbock K, Nothwang HG, Hu J, Hell JW, Schimmang T, Rüttiger L & Knipper M. (2013). L-type CaV1.2 deletion in the cochlea but not in the brainstem reduces noise vulnerability: implication for CaV1.2-mediated control of cochlear BDNF expression. Frontiers in Molecular Neuroscience 6.

Zuo H, Cui B, She X & Wu M. (2008). Changes in Guinea pig cochlear hair cells after sound conditioning and noise exposure. J Occup Health 50, 373–379. [PubMed: 18654041]

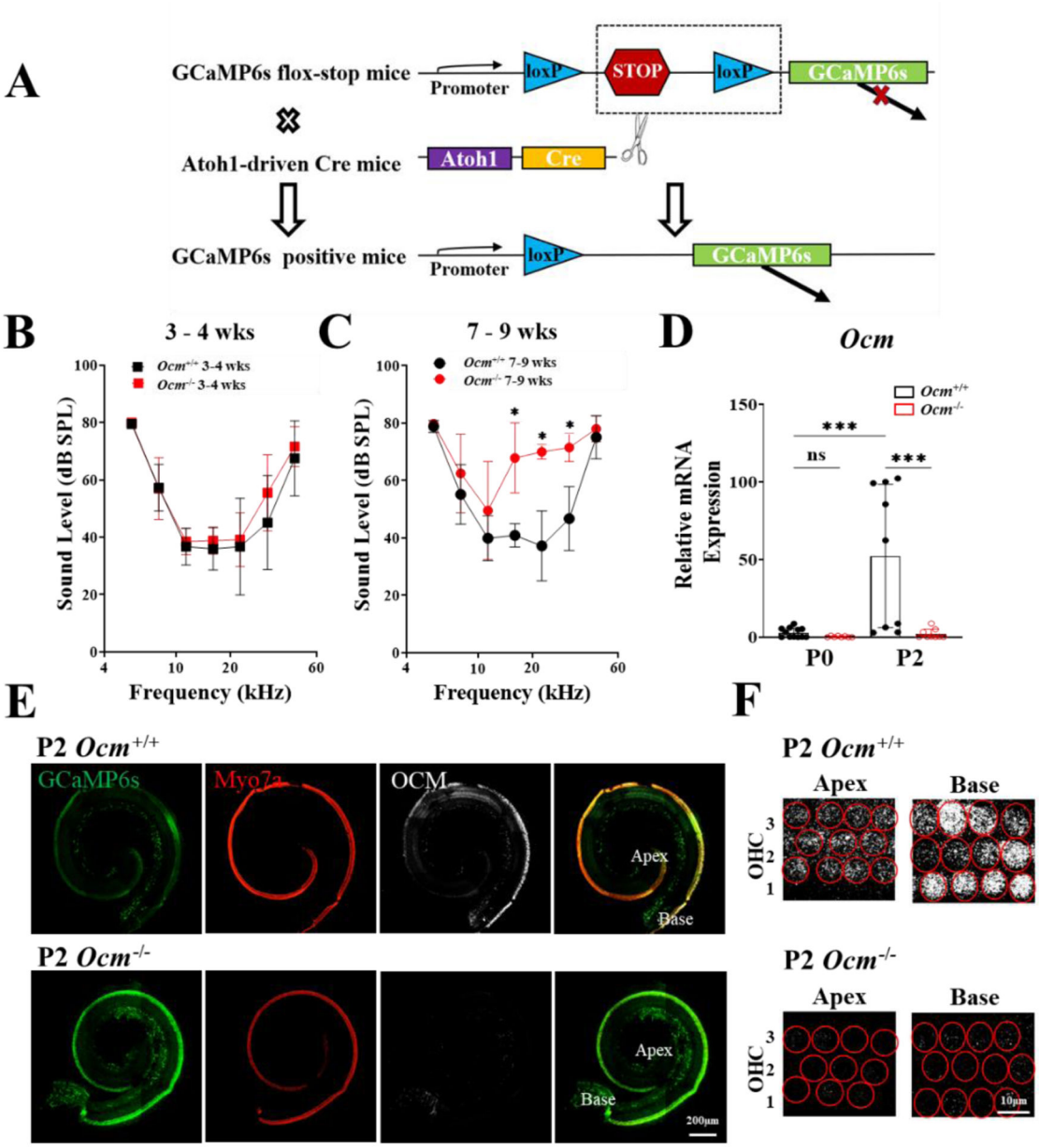

Figure 1. OCM expression in GCaMP6s mice can be detected as early as P2.

A, Schematic showing generation of *Atoh1*-driven, GCaMP6s $Ocm^{+/+}$ and $Ocm^{-/-}$ mice. Ai96 mice (see Methods) contain a floxed-STOP cassette preventing transcription of the GCaMP6. After crossing with *Atoh1*-Cre mice, the floxed-STOP cassette was removed, leading to a tissue-specific expression of GCaMP6s in the inner ear region. **B-C**, Distortion product otoacoustic emissions (DPOAEs) were measured from 3 – 4 weeks (wks) and 7–9 wks $Ocm^{-/-}$ (8 and 5 mice, respectively) and aged-matched $Ocm^{+/+}$ mice (6 and 11 mice). For 3 – 4 wks, $P = 0.543$, *two-way ANOVA*, $P = 0.984$ at 5 kHz, $P > 0.999$ at 8 kHz, $P = 0.990$ at 11 kHz, $P = 0.980$ at 16 kHz, $P = 0.872$ at 22 kHz, $P > 0.999$ at 32 kHz, $P = 0.987$ at 45 kHz, *Bonferroni* post test. For 7 – 9 wks, $P = 0.007$, *two-way ANOVA*, $P = 0.634$ at 5 kHz, $P = 0.982$ at 8 kHz, $P = 0.894$ at 11 kHz, $P = 0.017$ at 16 kHz, $P = 0.040$ at 22 kHz, $P =$

0.020 at 32 kHz, $P = 0.998$ at 45 kHz, *Bonferroni* post test, *two-way ANOVA*. **D**, qRT-PCR results of *Ocm* mRNA expression from the cochlea of $Ocm^{+/+}$ and $Ocm^{-/-}$ mice at postnatal day 0 (P0) and P2. Results are normalized to $Ocm^{+/+}$at P0. $P < 0.001$, *one-way ANOVA*. *Bonferroni post*-test: $P > 0.999$ for P0 $Ocm^{+/+}$ vs. P0 $Ocm^{-/-}$, $P < 0.001$ for P2 $Ocm^{+/+}$ vs. P2 $Ocm^{-/-}$ and P0 $Ocm^{+/+}$ vs. P2 $Ocm^{+/+}$. 4 and 3 $Ocm^{+/+}$ mice for P0 and P2, 3 $Ocm^{-/-}$ mice at both ages. 3 replicas for each animal group, no *Ocm* mRNA was detected from one of the P0 $Ocm^{-/-}$replications. **E-F,** Gradient expression of OCM along the tonotopic axis at P2. Maximum intensity projection images taken from the apical-cochlea of $Ocm^{+/+}$ and $Ocm^{-/-}$ mice at P2. Cochleae showed endogenous green fluorescence (green). OCM (white) expression can be detected in P2 $Ocm^{+/+}$ mice, and exhibited a gradient expression along the cochlear coil, with a higher level at the base and lower at the apex (n = 3). Myo7a (red) was used as the hair cell marker.

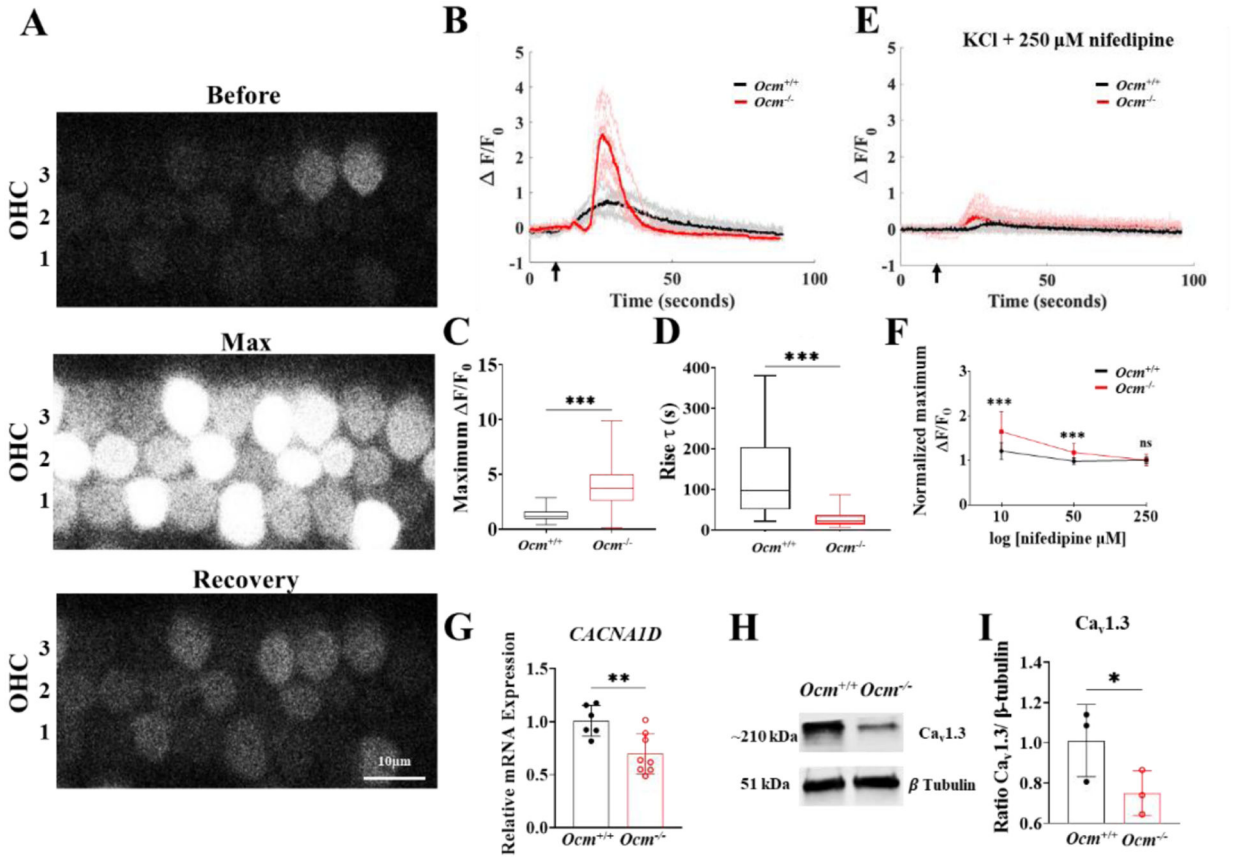

Figure 2. The absence of OCM increased the fractional change of voltage-gated Ca^{2+} influx in OHCs.

A, Organ of Corti were taken from GCaMP6s mice at P2. KCl (37 mM final concentration) superfusion was administered to elicit Ca^{2+} transients. GCaMP6s fluorescence is shown before the superfusion of KCl (top), at peak response (middle), and the recovery stage (bottom). Recordings were taken at room temperature (~24°). Representative Ca^{2+} transient images taken from the cochlear apex of *Ocm*$^{-/-}$ P2 mice. **B,** Representative plots of GCaMP6s fluorescence fractional change ($\Delta F/F_0$) in OHCs induced by KCl superfusion (arrow). Results show individual ROI fluorescence $\Delta F/F_0$ traces view (grey and light red) and mean $\Delta F/F_0$ for OHCs (black and red) from P2 *Ocm*$^{+/+}$ and *Ocm*$^{-/-}$ mice. **C,** Average maximum fluorescence intensities from OHCs of P2 *Ocm*$^{+/+}$ and *Ocm*$^{-/-}$ mice during the application of KCl. Mean peak $\Delta F/F_0$ are plotted from single OHCs in all 3 rows (39 OHCs from 4 *Ocm*$^{+/+}$ mice, 208 OHCs from 6 *Ocm*$^{-/-}$, $P < 0.001$, *t*-test). **D,** Rise τ from OHCs of P2 *Ocm*$^{+/+}$ and *Ocm*$^{-/-}$ mice during the application of KCl (20 OHCs from 4 *Ocm*$^{+/+}$ mice, 73 OHCs from 6 *Ocm*$^{-/-}$, $P < 0.001$, *Mann-Whitney* test). **E,** Individual ΔF/F0 traces (grey and light red) and mean ΔF/F0 (black and red) from *Ocm*$^{+/+}$ and *Ocm*$^{-/-}$ OHCs induced by the KCl application (arrow) with the presence of 250 μM nifedipine. **F,** Normalized maximum $\Delta F/F_0$ showing the effect of nifedipine on KCl-induced Ca^{2+} transients in OHCs from *Ocm*$^{+/+}$ and *Ocm*$^{-/-}$ P2 mice. Cochlear explants were incubated with 10 μM, 50 μM, and 250 μM nifedipine before KCl perfusion. Relative peak $\Delta F/F_0$ from different nifedipine dosage treatments were normalized to average peak $\Delta F/F_0$ when 250 μM

nifedipine was applied. X-axis: logarithm of nifedipine concentration. $P < 0.001$, two-*way ANOVA*, *Bonferroni* post test: $P < 0.001$ for 10 μM nifedipine, 43 OHCs from 2 $Ocm^{+/+}$ and 68 OHCs from 2 $Ocm^{-/-}$ mice; $P < 0.001$ for 50 μM nifedipine, 34 OHCs from 2 $Ocm^{+/+}$ and 95 OHCs from 2 $Ocm^{-/-}$ mice; $P > 0.999$ for 250 μM nifedipine, 28 OHCs from 2 $Ocm^{+/+}$ and 81 OHCs from 2 $Ocm^{-/-}$ mice. **G,** qRT-PCR results of $Ca_v1.3$ (*CACNA1D*), 6 replicas from 3 $Ocm^{+/+}$ and 8 replicas from 3 $Ocm^{-/-}$ mice at P2. Plots are normalized mRNA levels relative to $Ocm^{+/+}$, $P = 0.0030$, *t*-test. **H-I,** Representative western blot for $Ca_v1.3$ protein expression levels detected in cochlea harvested from P2 $Ocm^{+/+}$ and $Ocm^{-/-}$ mice. Each genotype has n = 3 independent repeats, each replicate contained 3 cochleae, total animal n = 9 for each genotype. *: $P = 0.0490$, *t*-test. β-tubulin (loading control) was used for normalization. The plot is normalized grey values relative to P2 $Ocm^{+/+}$ mice.

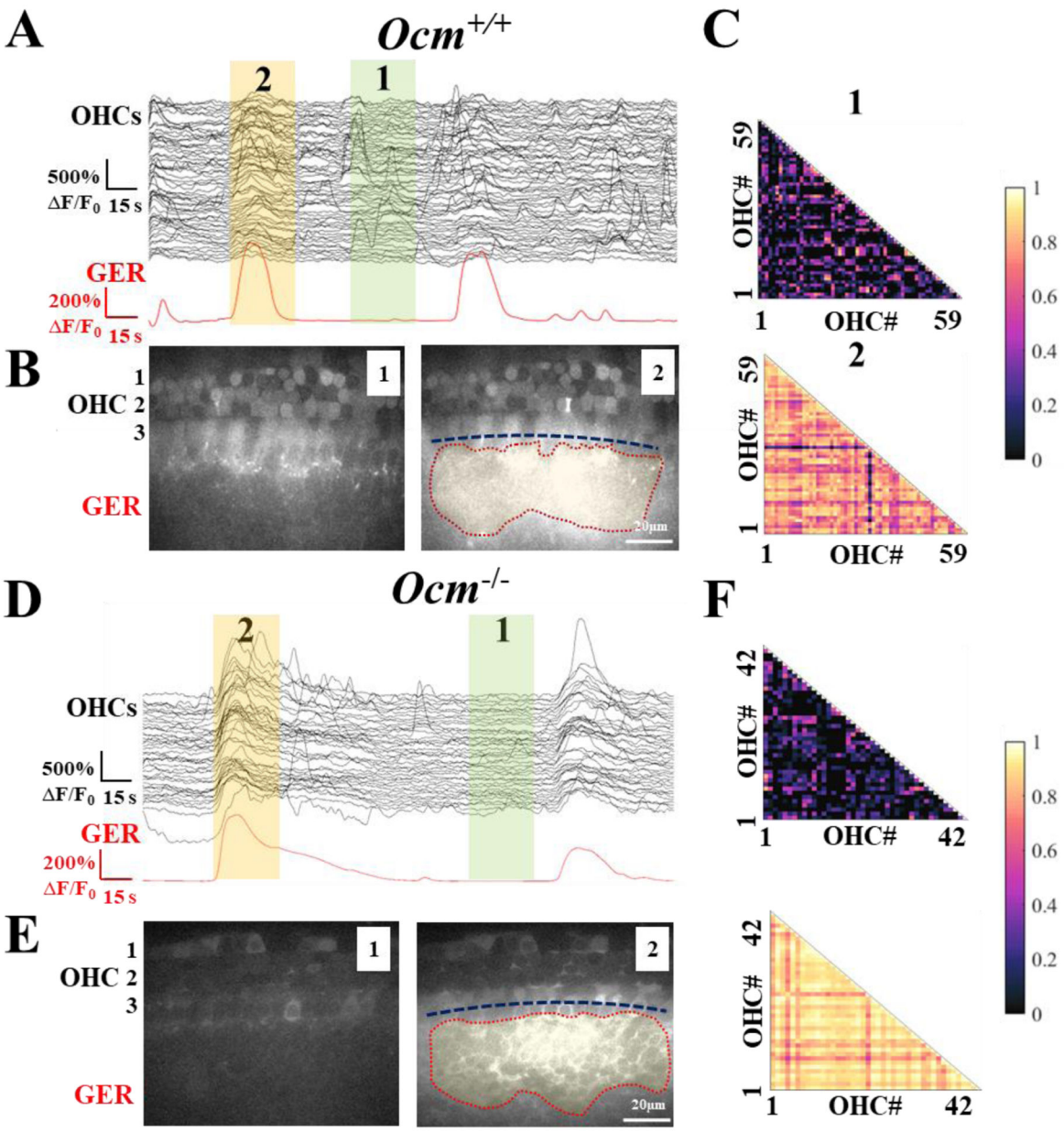

Figure 3. Ca^{2+} waves initiated from the GER synchronized spontaneous Ca^{2+} activities in *Ocm*$^{+/+}$ and *Ocm*$^{-/-}$ OHCs

A, D, Apical coil of the cochleae taken from GCaMP6s mice at P2. Individual ROI GCaMP6s fluorescence intensity are shown as fractional change ($\Delta F/F_0$) traces for all OHCs from a single field of view (black), and Ca^{2+} activity in GER (red). Highlighted green time window (1) represents no Ca^{2+} wave in GER. In contrast, the yellow time window (2) marks the occurrence of a Ca^{2+} wave in GER. Recordings were taken at ~24°. **B, E,** Representative images taken from time windows 1 (green) and 2 (yellow) showing the background and the occurrence of the Ca^{2+} waves in GER for *Ocm*$^{+/+}$ and *Ocm*$^{-/-}$ cochlea, respectively. Dash lines represent the extension size of the Ca^{2+} wave in GER along the cochlear spiral. **C, F,** Representative correlation matrices of $\Delta F/F_0$ traces in OHCs. Correlation matrices were computed during time window 1 (top panel), and time window 2 (bottom panel). Each

matrix element represents Spearman's rank correlation coefficient (r_s, see Materials and Methods) of one pair of OHCs from the same cochlear spiral.

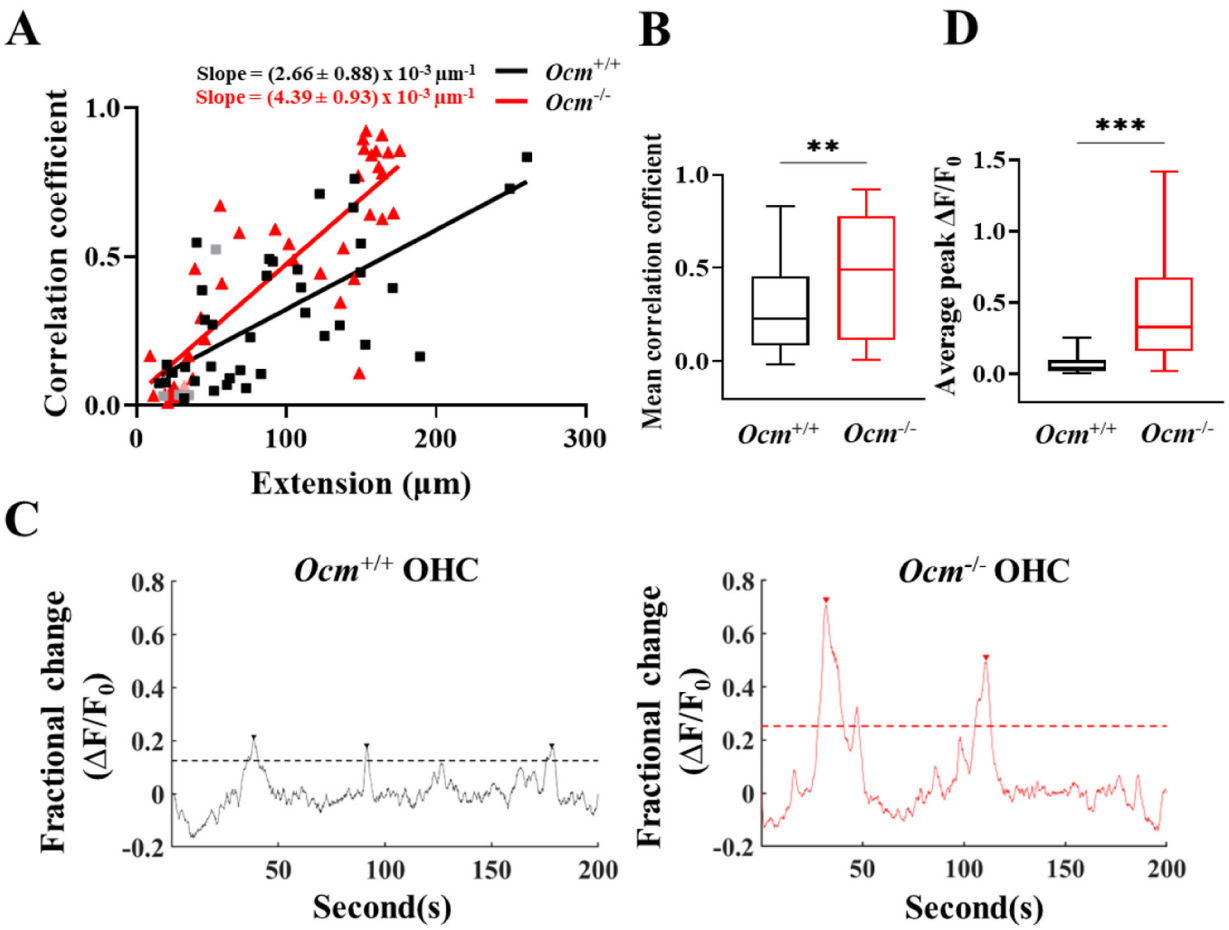

Figure 4. $Ocm^{-/-}$ OHCs exhibited a higher level of correlated Ca^{2+} activity and increased maximum $\Delta F/F_0$ during the Ca^{2+} waves initiated in the GER.

A, The linear regression between the longitudinal extension of spontaneous Ca^{2+} waves in GER and the average Spearman's rank correlation coefficient (r_{avg}, see Materials and Methods) of OHCs from $Ocm^{+/+}$ and $Ocm^{-/-}$ apical cochlea. Black and red dots symbols represent a significant increase in pairwise OHCs correlation ($P < 0.050$, *Mann-Whitney U*-test) compared to their background time window. Grey and light red symbols represent the correlation did not increase significantly. The slope rates were shown and were significantly different from zero ($P < 0.001$ for both $Ocm^{+/+}$ and $Ocm^{-/-}$ OHCs, *t*-test). $Ocm^{+/+}$: 44 Ca^{2+} waves, 11 cochleae and 8 mice; $Ocm^{-/-}$: 42 Ca^{2+} waves, 11 cochleae and 6 mice. **B,** Average correlation coefficient between the extension size of Ca^{2+} wave in GER and the r_{avg} in OHCs during the Ca^{2+} waves calculated from above. ns: no significance, $P = 0.006$, *Mann-Whitney* test. Number of waves, cochleae and mice as listed in panel A. **C,** Representative Ca^{2+} signaling in single OHC from $Ocm^{+/+}$ and $Ocm^{-/-}$ apical cochleae. Arrow represents a Ca^{2+} spike in OHC and only spikes that exceeded the threshold (dash line) were measured (see Materials and Methods).**D,** Average maximum $\Delta F/F_0$ of OHCs spontaneous Ca^{2+} activity. $P < 0.001$, *Mann-Whitney* test. $Ocm^{+/+}$: 2171 Ca^{2+} spikes in OHCs from 11 cochleae; $Ocm^{-/-}$: 2198 Ca^{2+} spikes in OHCs from 11 cochleae.

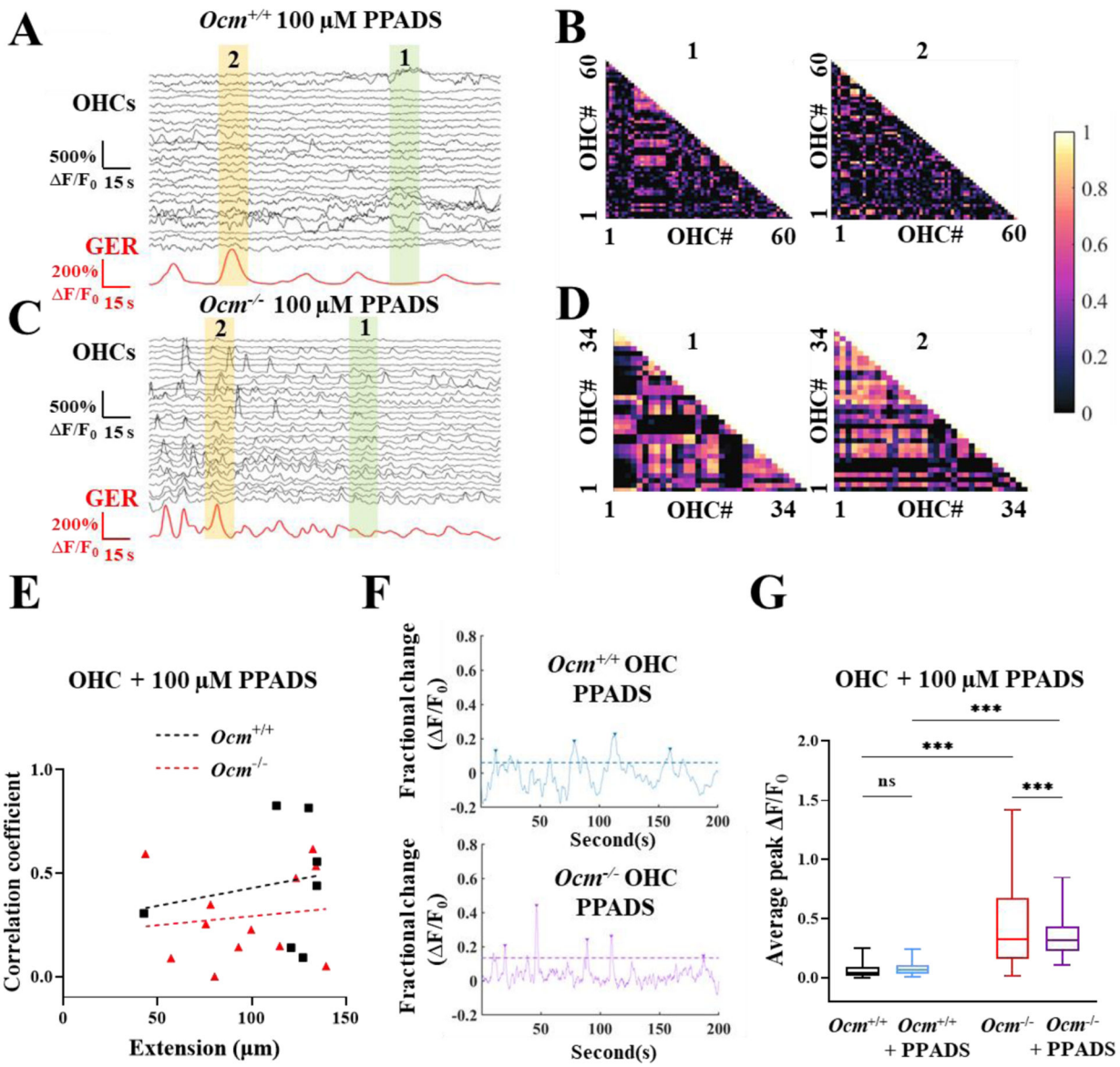

Figure 5. The purinergic receptor is required for the synchronization of spontaneous Ca^{2+} activity.

A-D, Individual ROI $\Delta F/F_0$ traces for all OHCs from a single field of view (black) and Ca^{2+} activity in GER (red) were taken from *Ocm*$^{+/+}$ and *Ocm*$^{-/-}$ mice at P2. Highlighted green (1) and yellow (2) time windows represent no Ca^{2+} wave (background), and the occurrence of Ca^{2+} wave in GER, respectively, and were used for correlation analysis. The right panel shows representative Ca^{2+} signaling in a single OHC. **B** and **D,** Representative correlation matrices calculated from **A** and **C** time window 1 (background, left panel) and time window 2 (during the occurrence of Ca^{2+} wave in GER, right panel). Each matrix element represents Spearman's rank correlation coefficient (r_s) of one pair of OHCs. **E,** The linear regression between the longitudinal extension of spontaneous Ca^{2+} waves in GER and the average Spearman's rank correlation coefficient (r_{avg}, see Materials and Methods) of OHCs from *Ocm*$^{+/+}$ and *Ocm*$^{-/-}$ apical cochlea with the continuous presence of PPADS (100 µM).

Ocm$^{+/+}$: 7 waves from 4 mice; *Ocm*$^{-/-}$: 12 waves from 3 mice. The slope from both *Ocm*$^{+/+}$ and *Ocm*$^{-/-}$ OHC showed no significant deviation from zero (*Ocm*$^{+/+}$: $P = 0.685$, *Ocm*$^{-/-}$: $P = 0.695$, *t*-test). **F, G,** Representative Ca^{2+} signaling in single OHC from *Ocm*$^{+/+}$ and *Ocm*$^{-/-}$ apical cochlea with the presence of PPADS (100μM). Arrow represents a Ca^{2+} spike in OHC, only spikes that exceeded the threshold (dash line) were calculated (see Materials and Methods). The average maximum $\Delta F/F_0$ of OHCs spontaneous Ca^{2+} activity with the presence or absence of PPADS was plotted. $P < 0.001$, *two-way ANOVA*. *Bonferroni* post test: $P = 0.651$ for *Ocm*$^{+/+}$ with or without PPADS, $P < 0.001$ for *Ocm*$^{-/-}$ with or without PPADS, $P < 0.001$ for *Ocm*$^{+/+}$ with PPADS and *Ocm*$^{-/-}$ with PPADS (3 mice for each genotype, 560 spikes from *Ocm*$^{+/+}$ OHCs and 588 spikes from *Ocm*$^{-/-}$OHCs).

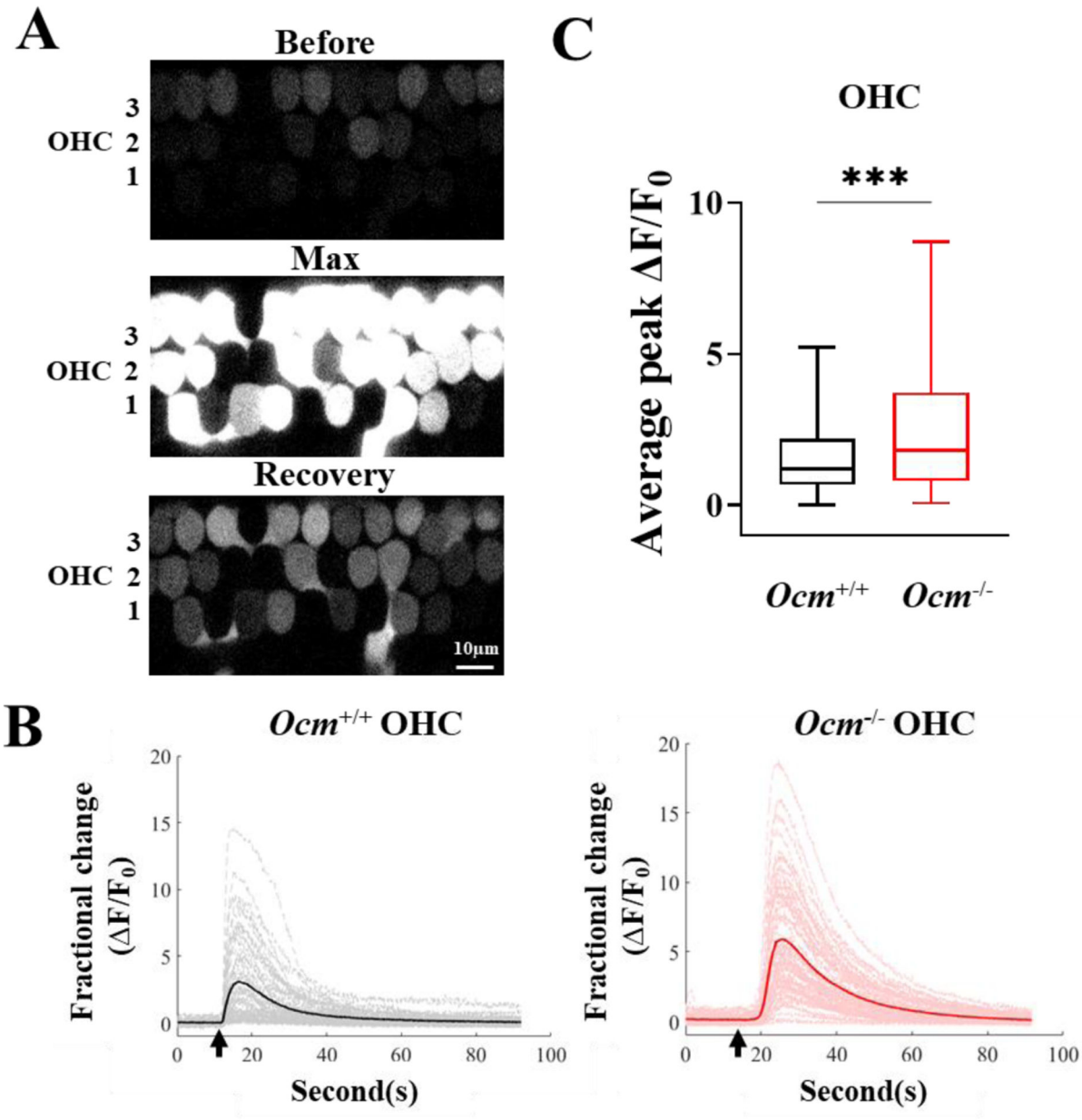

Figure 6. ATP-induced Ca^{2+} transients are altered in *Ocm*$^{-/-}$ mice.

A, Representative images of Ca^{2+} transients in OHCs from P2 *Ocm*$^{-/-}$ mice shown before 200 μM ATP superfusion, at peak response, and the recovery stage. **B,** Representative plots of the fractional change ($\Delta F/F_0$) in GCaMP6s fluorescence induced by 200 μM ATP superfusion (arrow). Results show individual ROI fluorescence $\Delta F/F_0$ traces view (grey and light red) and mean $\Delta F/F_0$ for OHCs from P2 *Ocm*$^{+/+}$ and *Ocm*$^{-/-}$ mice. **C,** Average maximum $\Delta F/F_0$ of OHCs from *Ocm*$^{+/+}$ and *Ocm*$^{-/-}$ mice at P2, induced by 200 μM ATP superfusion. $P < 0.001$, *Mann-Whitney* test, 119 OHCs from 4 *Ocm*$^{+/+}$ mice, 325 OHCs from 7 *Ocm*$^{-/-}$ mice.

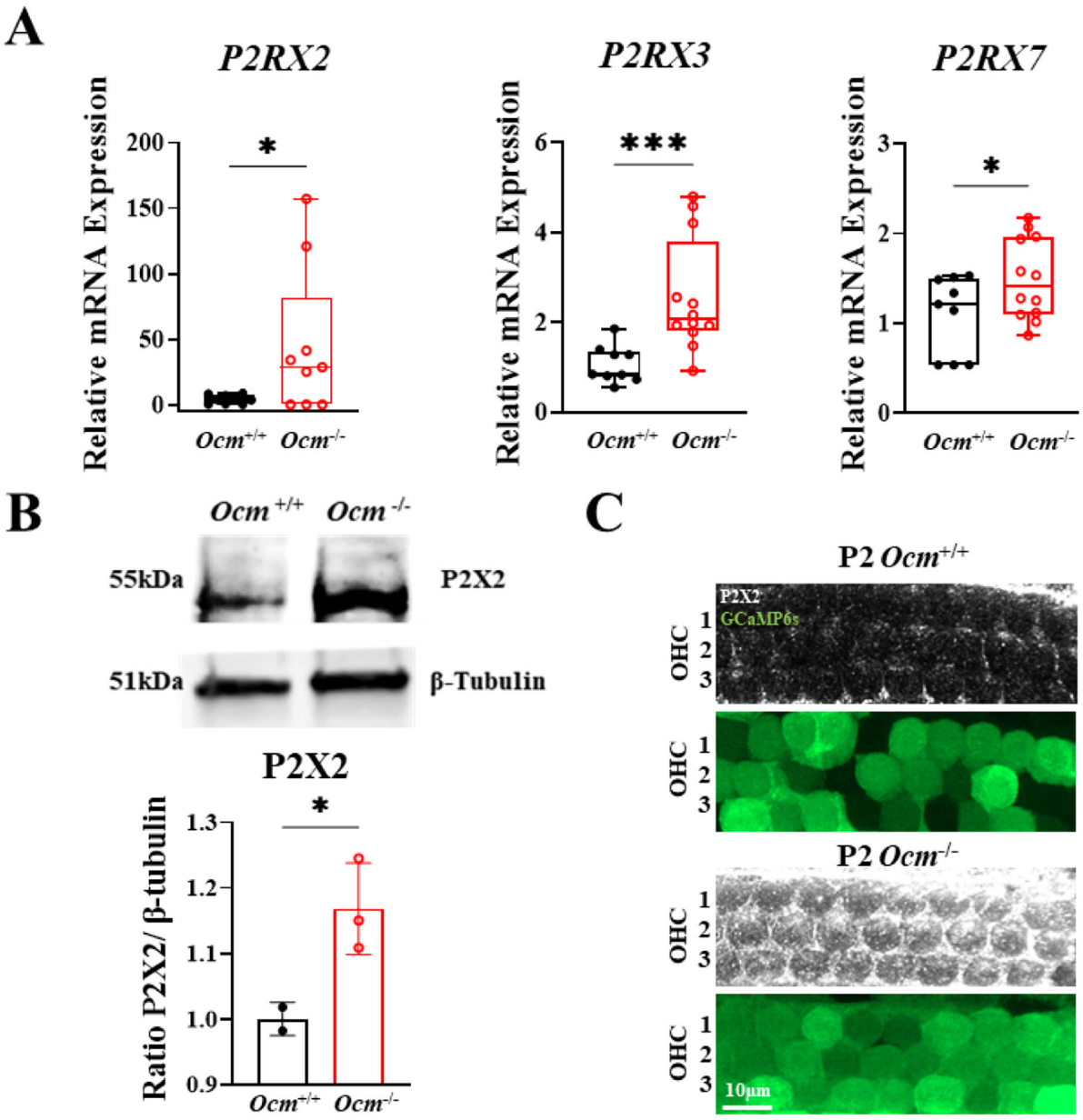

Figure 7. P2X purinoceptor 2 (P2X2) expression is upregulated in *Ocm*$^{-/-}$ mice

A, qRT-PCR results show that *P2RX2*, *P2RX3,* and *P2RX7* relative expression level is significantly increased in the cochlea of P2 *Ocm*$^{-/-}$ mice compared to littermate controls. For *P2RX2*, 9 replicas from 3 animals for each genotype. For *P2RX3* and *P2RX7*, 9 replicates from 3 animals for *Ocm*$^{+/+}$, 12 replicates from 4 animals for *Ocm*$^{-/-}$. All values were normalized to *Ocm*$^{+/+}$. $P = 0.021$ for *P2RX2*, $P < 0.001$ for *P2RX3*, $P = 0.028$ for *P2RX7*. **B,** Representative western blot for P2X2 expression levels detected in cochlea derived from P2 *Ocm*$^{+/+}$ and *Ocm*$^{-/-}$ mice. β-tubulin (loading control) was used for normalization. 2 replicates for *Ocm*$^{+/+}$, 3 replicates for *Ocm*$^{-/-}$, each one containing 3 mice cochlear spirals. Plot is normalized grey values relative to *Ocm*$^{+/+}$. $P = 0.026$, *t*-test. **C,** Maximum intensity projections of P2X2 immunolabeling on three rows of OHCs harvested

from P2 *Ocm*$^{+/+}$ and *Ocm*$^{-/-}$ mice, n = 3 for each genotype. P2X2 (white), and GCaMP6s (green) are shown.

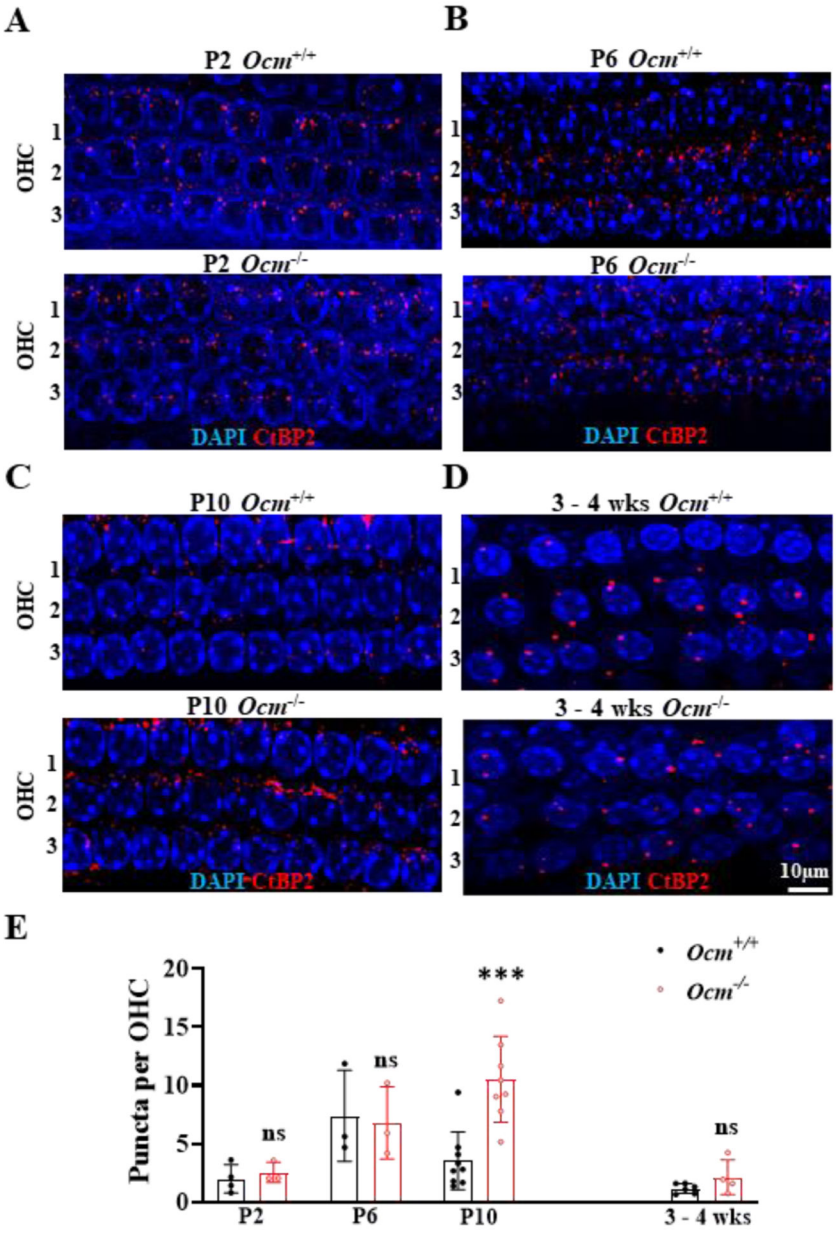

Figure 8. Ribbon synapse maturation is delayed in *Ocm*$^{-/-}$ mice.

A-D, Maximum intensity projections of confocal z-stacks from *Ocm*$^{+/+}$ and *Ocm*$^{-/-}$ apical cochlea at P2, P6, P10, and 3 – 4 wks. Three rows of OHCs with ribbon synapses (CtBP2, red) and DAPI (blue) are shown. **E,** The average number of ribbon synapses puncta per OHC from the apical cochlea was measured. The CtBP2 puncta within 4 μm of the OHC nuclei were counted. Bar graphs show the number of ribbons per OHC. $P = 0.004$, *two-way ANOVA*. *Bonferroni* post test: At P2, $P > 0.999$, 4 *Ocm*$^{+/+}$ and 3 *Ocm*$^{-/-}$ mice. At P6, $P > 0.999$, 3 *Ocm*$^{+/+}$ and 3 *Ocm*$^{-/-}$ mice. At P10, $P < 0.001$, 9 *Ocm*$^{+/+}$ and 8 *Ocm*$^{-/-}$ mice. At 3 – 4 wks, $P > 0.999$, 6 *Ocm*$^{+/+}$ and 4 *Ocm*$^{-/-}$ mice.

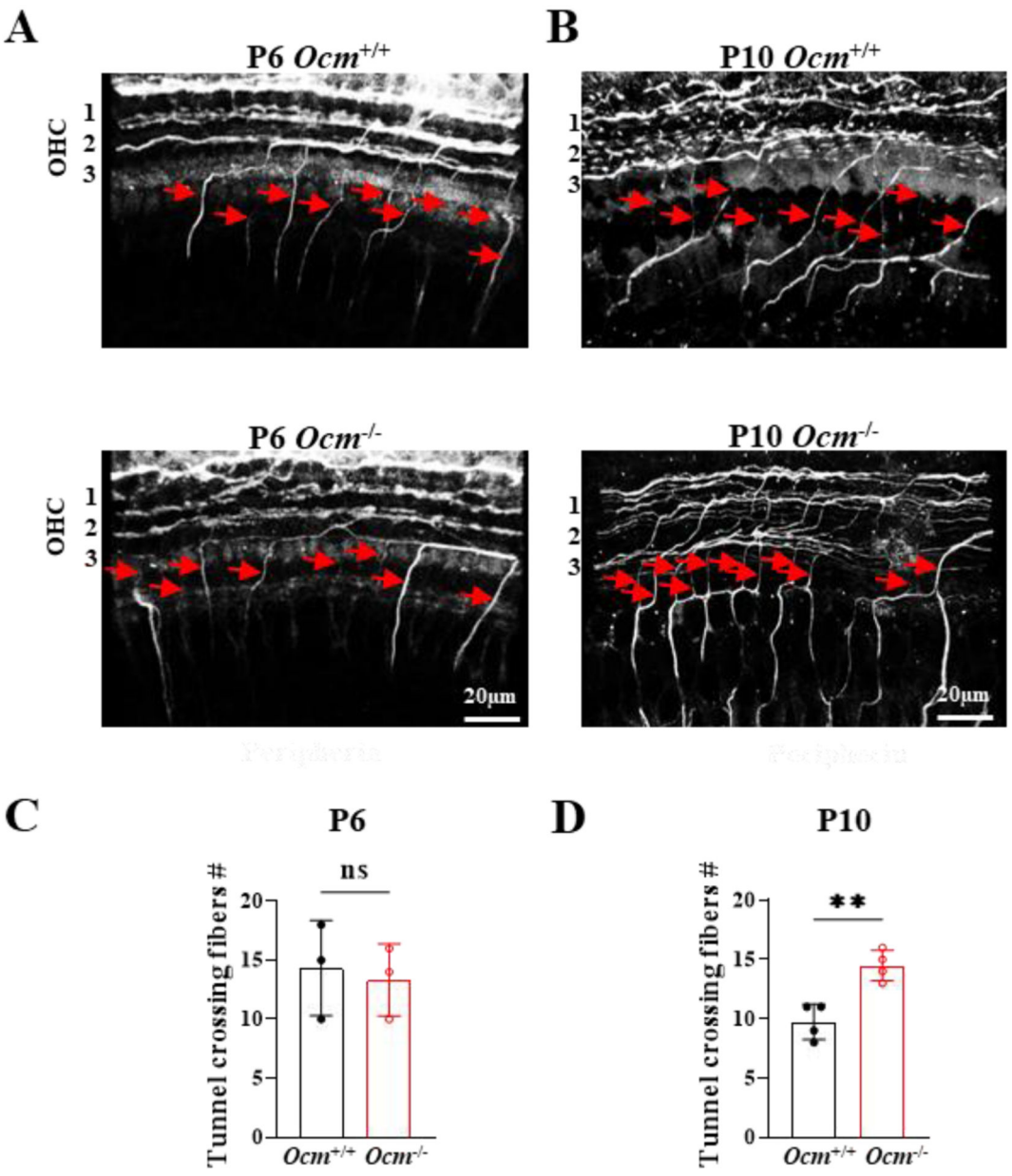

Figure 9. Afferent fibers increased in *Ocm*$^{-/-}$ at P10

A, B, Maximum intensity projections of confocal z-stacks from the apical coil of the cochlea of *Ocm*$^{+/+}$ and *Ocm*$^{-/-}$ mice at P6 and P10. Afferent fibers labeled with peripherin (white) and DAPI (blue) are shown. The outer spiral fibers of type II spiral ganglion neurons travel toward the cochlear base (arrows). **C, D**, The average number of tunnel crossing afferent fibers from mice of both genotypes at P6 and P10. At P6, 3 animals for each genotype, $P = 0.375$, *t-test.* At P10, 4 animals for each genotype, $P = 0.002$, *t-test.*

Movie 1.

Representative movie shows KCl-induced Ca^{2+} transient in OHCs.

Movie 2.

Representative movie shows spontaneous Ca^{2+} activity in GCaMP6s cochlea after acute preparation.

Movie 3.
Representative movie shows extracellular ATP-induced Ca^{2+} transient in OHCs.